

# Development and Simulation of Damage Tolerant Control Laws for a Compound Helicopter

Marit E. Knapp \*

*San Jose State University Research Foundation, Ames Research Center, Moffett Field, CA*

Christina M. Ivler †

*University of Portland, Portland, OR*

Joseph F. Horn ‡

Eric N. Johnson §

*The Pennsylvania State University, University Park, PA*

Derek O. Bridges ¶

*Piasecki Aircraft Corporation, Essington, PA*

Mark J. S. Lopez||

Mark B. Tischler \*\*

*CCDC AvMC Aviation Development Directorate, Moffett Field, CA*

Joseph A. Wagster††

Kenny K. Cheung ‡‡

*Universities Space Research Association, Ames Research Center, Moffett Field, CA*

A piloted simulation study was conducted to evaluate damage tolerant control (DTC) law concepts. The simulated aircraft is a fly-by-wire compound utility helicopter based on the X-49A. The aircraft features auxiliary thrust through a vectored thrust ducted propeller and auxiliary lift through a wing. The configuration includes a number of redundant control surfaces, including flaperons and elevators that help enable DTC. This paper covers the design of the baseline inner-loop control laws, which were optimized to meet Level 1 requirements for a comprehensive set of stability, handling qualities and performance specifications. Methodology and development of the control allocation methods for DTC is presented. The fixed-base piloted simulation experiment qualitatively and quantitatively evaluated the baseline control laws with various control allocation methods. Handling qualities ratings were collected using a series of maneuvers, including pitch and roll capture and tracking tasks. Survivability ratings, quantitative performance metrics, and pilot comments were collected for multiple damage scenarios in which the pilot attempted to safely land the aircraft following damage that severely limited control in one or more axes. Handling qualities ratings were also collected for the tracking tasks in the presence of damage. The paper is concluded with an overall evaluation and comparison of the damage tolerant methods.

---

\*Research Engineer, Member AIAA

†Assistant Professor of Mechanical Engineering, Member AIAA

‡Professor of Aerospace Engineering, Associate Fellow AIAA

§Professor of Aerospace Engineering, Associate Fellow AIAA

¶Project Engineer, Senior Member AIAA

||Aerospace Engineer, U.S. Army Aviation and Missile Center, Member AIAA

\*\*Flight Control Technology Group Leader, Senior Technologist, U.S. Army Combat Capabilities Development Command Aviation & Missile Center, Associate Fellow AIAA

††Former USRA Research Engineer (2017)

‡‡Chief Software Architect

Distribution Statement A: Approved for public release; distribution is unlimited.

## Nomenclature

$\alpha$	Angle of attack	cal	
$\beta$	Sideslip angle	$g$	Gravity
$\Delta d$	Commanded change in control force/moment	$J$	Cost
$\delta_{lat}, \delta_{lon}, \delta_{col}, \delta_{ped}$	Pilot inputs: lateral and longitudinal cyclic stick, collective, and pedals	$n_\omega$	Number of frequency points
$\delta_{servo}, \delta_{rud}, \delta_{elev}, \delta_{flap}$	Aero-surface inputs: Main rotor servos, rudder servo, elevators, flaperons	$p, q, r$	Angular rates: roll, pitch, yaw
$\gamma_{xy}^2$	Coherence	<i>pref</i>	Preferred
$\omega_c$	Crossover frequency	$u$	Control actuator inputs
$\Phi, \Theta, \Psi$	Total (absolute) attitudes: roll, pitch, yaw	$V_{tot}$	Total velocity
$\phi, \theta, \psi$	Perturbation attitudes: roll, pitch, yaw	$x$	Aircraft states vector
$A, B, C, D$	State-space matrices	$Y_c$	Aircraft model
$I$	Identity matrix	$Y_p$	Pilot model
$W$	Weighting matrix	$Y_p Y_c$	Pilot-vehicle system
$\tau_\theta$	Equivalent time delay	ave, std dev	Average, standard deviation
$a_x, a_y, a_z$	Accelerations: longitudinal, lateral, vertical	BL	Broken-loop response
		cm, <i>cmd</i>	Command model or value
		GM, PM	Gain and phase margin
		min, max	Minimum, maximum value
		RMS	Root mean squared value

## I. Introduction

MODERN aircraft will fly further and faster, with better reliability and survivability, and have the ability to operate in Degraded Visual Environments (DVE).<sup>1-4</sup> In recent years, a crisis point has been reached with hundreds of rotorcraft and lives lost during military operations.<sup>5</sup> Therefore, rotorcraft in the Future Vertical Lift (FVL) program will be built to achieve superior survivability through both the airframe and control system design. Unlike conventional aircraft flight control systems which feature a single control effector for the roll, pitch, and yaw degrees of freedom, advanced rotorcraft configurations introduce additional control effectors, possibly including both traditional rotorcraft controls (rotor cyclic and collective), as well as fixed-wing control surfaces (ailerons, elevators, flaps, and propeller pitch).<sup>6</sup>

A major advantage to having multiple control surfaces, is the redundancy and ability to reconfigure for damage. Envision a scenario where a main rotor servo locks up on a winged compound helicopter. In such an aircraft, the number of control surfaces is greater than the number of control parameters (overactuated), so instead of the pilot compensating for the uncommanded roll (or worse, losing control of the aircraft), the control system could re-allocate the elevators and flaperons to stabilize the aircraft. This scenario would not generally be possible on a conventional helicopter that does not have multiple/redundant surfaces to produce the necessary control effect.

Additional control surfaces not only provide great potential for improved survivability, but also improved performance, which is contingent on the flight control system. To control an overactuated aircraft, the control system typically uses a control allocation scheme. The control laws specify the total forces and moments to produce, and the control allocation distributes this control requirement among the individual surfaces. The control allocation determines which surfaces to use and in what proportion. To reduce pilot workload<sup>7</sup> and deploy the control effectors in an optimal manner, these decisions are best determined by the flight control laws. Due to the unstable and coupled nature of rotorcraft, this is a challenging problem.

Different techniques of accomplishing control allocation are: control ganging,<sup>8,9</sup> variations of inverse methods,<sup>8-10</sup> linear and quadratic programming<sup>8,11</sup> and others. The way in which the control allocation is designed affects the traditional flight performance of the aircraft. If control allocation is designed improperly, it could cause the actuators to saturate, reducing performance. This study leveraged prior research by Ref. 8, which evaluated numerous control allocation methods for a notional tilt rotor. There are key differences in the research. For example, a nonlinear blade element model was used for this research, adding additional levels of non-linearity and uncertainty, whereas only a linear model was used in the prior tilt-rotor work. Also, this study focuses on control allocation for failure reconfiguration, which was not addressed in the tilt-rotor study. However, Ref. 8 provides important insights on the trade-offs between control allocation methods and metrics

for evaluation of control allocation performance. The results showed that the pseudo-inverse method was the most robust to uncertainty, and the quadratic programming method provided handling qualities benefits associated with reduced actuator rate limiting.<sup>8</sup> This demonstrates the significant effect control allocation has on performance, and for this reason, selecting a robust and optimal method of control allocation is crucial.

This research explored advanced damage tolerant control (DTC) systems that are adaptive and re-allocate for damage. An explicit model following architecture for the inner-loop control laws was designed to serve as the baseline controller for the advanced rotorcraft simulation model. Two types of damage tolerant components were then developed and added to the baseline controller: the control allocation and an adaptive neural network element. The pseudo inverse and quadratic programming control allocation schemes were designed to re-allocate the individual control surfaces based on a known damage condition. The neural network adaptive controller adjusts the feedback compensation to better track commands in the presence of damage or other model uncertainties. A simulation of a winged compound rotorcraft, the X-49A, was used as the demonstration vehicle to test the damage tolerant controllers.

Piasecki Aircraft Corporation (PiAC) developed its X-49A winged compound helicopter with funding from a demonstration contract with the U.S. Army Aviation Applied Technology Directorate (AATD).<sup>12</sup> The over 86 hour flight test program of the X-49A, demonstrated the potential for an advanced rotorcraft design with an advanced flight control system to achieve significant improvements in performance, safety, survivability and life-cycle costs over conventional helicopters.<sup>13</sup> In 2014, PiAC began to develop a rotorcraft-based adaptive flight control system, named Adaptive Digital Automated Pilotage Technology (ADAPT). ADAPT would enable the inherent redundancy of advanced VTOL platforms to achieve improvements in performance, safety/survivability and affordability. In 2016, PiAC was awarded a contract through the U.S. Army U.S. Army Combat Capabilities Development Command Aviation & Missile Center Aviation Development Directorate (CCDC AvMC ADD) to develop the ADAPT technology and carried the program through its first piloted simulation session.<sup>14,15</sup> The development of the technology has continued through a number of piloted simulation events and flight testing of a scale model demonstrator. Ultimately autonomous sub-scale flight test of ADAPT is envisioned based on a winged compound helicopter similar to the X-49A.

The research objective herein was to determine the best DTC system to continue maturation of the ADAPT technology. This selection was made based on pilot ratings and comments, overall flying performance, and damage tolerance capabilities from a piloted simulation including three of the recently created Mission Task Elements (MTEs) for evaluation of high speed flying performance.<sup>16-19</sup> This paper covers the development of the inner-loop control laws and damage tolerant components, integration of the control system elements, and validation of the implementation. Details of the simulation experiment set-up, along with how the damage is modeled are described. The remainder of the paper covers simulator test results, followed by discussion and conclusions.

## II. Simulation Model

### A. Aircraft Model

#### 1. Aircraft Description

For this work, the X-49S simulation model was used as the platform to assess the damage tolerant flight control system. The X-49S is representative of the X-49A compound helicopter that was developed, built and flight-tested by PiAC, shown in Figure 1. A SH-60F Seahawk helicopter was modified by adding a 30-foot span, low mid-fuselage wing with full-span flaperons to the airframe. The conventional tail rotor and stabilator of the Seahawk were replaced with a Vectored Thrust Ducted Propeller (VTDP) system. The VTDP consists of an aerodynamic duct, five-bladed variable-pitch propeller mounted on a propeller bearing box, two retractable sectors (made up of sections of a sphere) in the right side of the duct and a rudder and two-section elevator mounted in the exit area of the duct for vectoring propeller mass flow. The VTDP vectors most of the flow in the port direction in hover and low speed to provide anti-torque. In high speed flight, the sectors are retracted with the anti-torque force being primarily generated by lift forces on the rudder, while most of the flow and thrust forces are directed along the longitudinal axis. The VTDP on the X-49A was equipped with two independently actuated elevators in the slip stream of the propeller. In addi-

tion to these elevators, the X-49S also has external elevator surfaces mounted on the outside of the VTDP (external elevators were not present on the X-49A). The combination of flaperons, elevators, and main rotor provide significant redundancy of control in the roll, pitch, and vertical axes when operating in forward flight.

## 2. GENHEL Model Description

The X-49S simulation model was built from the GENHEL simulation of the UH-60A.<sup>20</sup> GENHEL uses a blade element representation of the main rotor with complete non-linear flap and lag dynamics. The Pitt-Peters 3-state inflow model is used to simulate induced velocities in the blade element rotor. GENHEL includes the full non-linear six degree of freedom fuselage equations of motion and uses numerous lookup tables for airframe, blade, and empennage aerodynamic coefficients. The simulation code was modified to incorporate a model of the VTDP that is largely based on test data from a 69% scale wind tunnel model and a full-scale ground test model of the VTDP system. A wing module with complete lift, drag, and moment coefficient lookup tables was also added. A combination of theoretical and empirical methods were used to develop models of interactional aerodynamics. Interactions between modules include rotor downwash corrections to VTDP and wing modules, wing downwash correction to the VTDP module, and wing blockage effects on the main rotor module during descent. The overall simulation was tuned based on X-49A flight test data,<sup>12</sup> and shown to match trim, frequency responses at hover, 70 kts, and 120 kts, and time response to simple pulse inputs at the same airspeeds.



Figure 1. Piasecki X-49A compound helicopter.

### B. Engine Model

GENHEL includes a comprehensive dynamic model of the T-700 engines as were used on the UH-60A Black Hawk with RPM regulation via Hydromechanical Unit coupled with an electronic Engine Control Unit. The SH-60F used an upgraded engine and controller relative to the UH-60A, but details of that system were not modelled. Instead, internal engine temperature limits were increased and the observed torque limits were adjusted to correspond to the SH-60F engines used on the actual X-49A. The X-49S is assumed to have a connection of the propeller pitch to the Load Demand System of the T-700 engine controller (to provide sufficient load anticipation when increasing propeller thrust). While this system has been designed, it was not actually flown on the X-49A.

### C. Flight Control System

The GENHEL model includes the detailed mechanical control gearing from pilot stick to the rotor blade controls. This contains the mechanical mixer (a mechanical system, designed to reduce coupling on the aircraft), mechanical linkages that convert pilot inputs to forward, aft, and lateral servo commands, with

primary servo models that have a 70 rad/sec bandwidth.

For the X-49S simulation, some of the control gearing terms were slightly modified to correspond to the SH-60F control gearing as published and measured on the actual X-49A.<sup>12</sup> One of the linkages of the mechanical mixer is assumed to be disabled - the pedal to longitudinal cyclic mixing. On the X-49A the link was still present (resulting in some undesirable yaw to pitch coupling), but a method for removing the link has been designed and assumed to be implemented on the X-49S. The X-49A included a mechanical mixing system to control the rudder, propeller pitch, and sector surfaces on the VTDP. This mixer (known as a walking beam), converts pilot pedal inputs and the pilot's propeller thrust command (controlled via a propeller BEEP switch) into appropriate combinations of surface deflections. The walking beam is non-linear such that the mapping of pedal inputs to rudder, sector, and propeller pitch changes substantially with flight condition as governed by the propeller beep. In hover / low speed mode, the rudder and sector are usually fully deflected, while pedals generate changes in propeller pitch that effectively change the anti-torque force. In high speed mode, the rudder deflects more linearly with pedal input, while the propeller pitch remains constant at the propeller beep setting.

The X-49A made use of the SH-60F Stability Augmentation System (SAS) in the roll and pitch axes. However, these systems are not used in the X-49S simulation as it is converted to full-authority Fly-by-Wire (FBW). Explicit model following control laws (as discussed below and in Ref. 21) were designed and implemented for the X-49S. The controllers are implemented in Simulink and then compiled to DLL that links with the GENHEL executable. The FBW system takes complete control of the surfaces of the VTDP, eliminating the need for the walking beam device discussed above. Instead, ideal mixing ("a virtual walking beam") is achieved via software in the control law.

#### D. Simulated Damage in GENHEL

The X-49S GENHEL model has been modified to allow for the introduction of a number of types of damage that military rotorcraft are particularly vulnerable to. The first three damage cases simulate the complete failure of either the forward, aft, or lateral main rotor servo actuator. When one of these damage cases is active, the damaged actuator is locked in place at a specified position, which prevents the swashplate from tilting freely as in normal operation. Instead, the swashplate is constrained to pivot at the connection to the damaged, locked-in-place actuator. The fourth damage case simulates damage to the VTDP on the tail section of the aircraft (as military rotorcraft are particularly susceptible to enemy fire on the empennage). The damage case simulates the removal of aft portions of the VTDP, including the duct, stators, elevators, and rudder, but not the propeller. The GENHEL model simulates the loss of mass at the tail, and aerodynamic effects from control surface loss. The metric used to quantify the amount of damage is rudder effectiveness relative to an undamaged aircraft, as this is the most prominent effect on handling qualities, but in fact the damage case simulates multiple physical effects such as a reduction in yaw stability and yaw inertia. The last damage case simulates propeller drive shaft failure.

#### E. X-49S Dynamic Characteristics

For development of the inner-loop control laws, linear, point models were extracted from the nonlinear GENHEL model from hover to 180 knots in increments of 20 knots. In studying the linearized point models, one can see that the dynamics change considerably with airspeed as shown in Figure 2. As the X-49S increases airspeed, its dynamics change from helicopter-like at hover, and take on more fixed-wing aircraft-like characteristics at high airspeeds. For example, this is most apparent when looking at the pitch response to main rotor  $q/\delta_{lon}$  in Figure 2, where the hovering cubic is apparent in the hover and 40 kt responses by the phase increase at low frequency, and this unstable behavior does not exist over 40 kts. From 1-12 rad/sec, the magnitude response changes from looking  $k/s$ -like to a constant magnitude that rolls off around 4 rad/sec as the aircraft's speed increases. Something similar occurs in the yaw axis, where the magnitude and phase responses of yaw rate to rudder  $r/\delta_{ped}$  have different behavior as airspeed is increased from around 40-80 kts. In the following section on control law design, these variations in dynamic characteristics will be addressed.

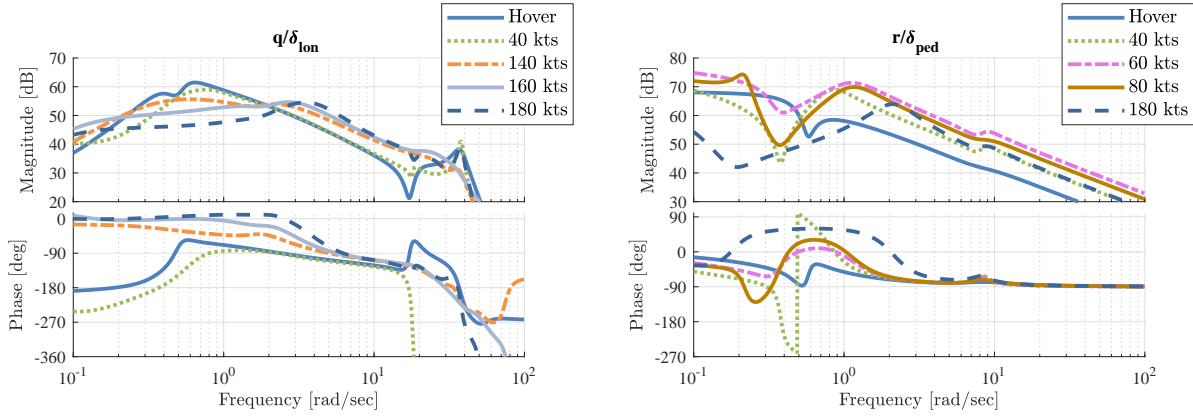


Figure 2. Comparison of X-49S frequency responses with airspeed in longitudinal ( $q/\delta_{lon}$ ) and directional axes ( $r/\delta_{ped}$ ).

### III. Control Laws

#### A. Explicit Model Following Control Law Architecture

An explicit model following control system architecture<sup>21</sup> was used as the base for X-49S work, as shown in perturbation block diagram form in Figure 3. Lookup tables are used to schedule inverse model parameters with airspeed, but these are not shown for simplicity. The main components of the explicit model following architecture are the Command Model, Equivalent Time Delay, Inverse Model and Feedback Compensation. The EMF architecture is designed to primarily use feed-forward compensation to follow the pilot commands (via the Command Model and Inverse Model), while minimizing the need for feedback when there are no external disturbances. The feedback gains can then be designed to provide required disturbance rejection, while meeting stability margin constraints.

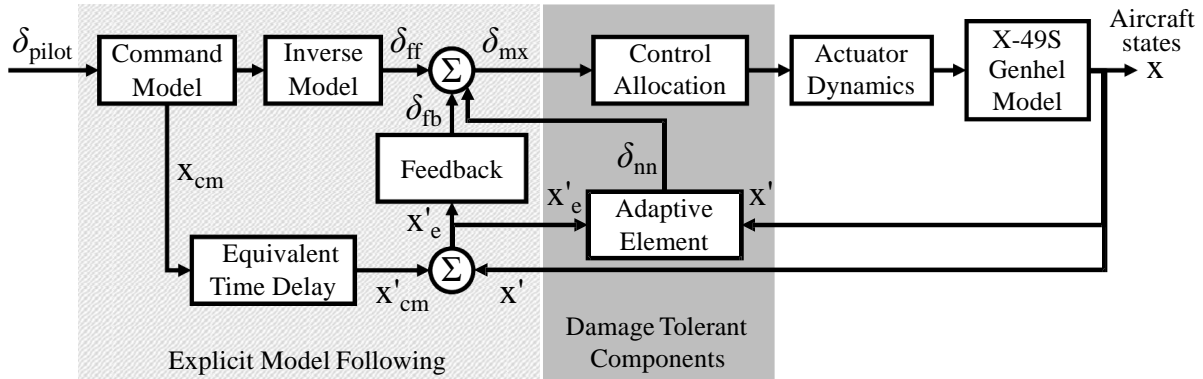


Figure 3. Perturbation block diagram of the control system with damage tolerant components.

##### 1. Command Model

This control architecture attempts to drive the system to match a lower-order command model that specifies the desired response to pilot inputs. The command model is designed to meet established handling qualities requirements in terms of response type and closed-loop bandwidth. For the present study, a first-order rate command response was used throughout the flight envelope. The command model parameters were set manually to meet the desired overall aircraft response to piloted inputs as according to the ADS-33E requirements for bandwidth.<sup>22</sup>

## 2. Inverse Model

The inverse model block, shown in Figure 3, takes the commanded rate responses of the aircraft and approximates the inputs needed to achieve the desired response (essentially generating feed-forward inputs). The inverse models are composed of lower-order equivalent system (LOES) approximations of the primary bare-airframe responses in the frequency range around crossover. Bare-airframe model simplification and decoupling was accomplished with the constrained variable approach using coupling numerators.<sup>23-25</sup> For the pitch rate  $q$  response, a simple first-order transfer function fit was used:

$$\frac{q}{\delta_{lon}} = \frac{M_{\delta_{lon}}}{s - M_q} \quad (1)$$

For the roll rate  $p$  and yaw rate  $r$  responses, a first-order transfer function fit was calculated for low airspeeds and a first/second-order transfer function fit was at high airspeeds. As described above, the dynamics of the X-49S change with airspeed, therefore from hover to  $\sim 130$  kts the aircraft behaves like a classic helicopter in pitch, which can be fit with a first-order transfer function. However, at high airspeeds, the X-49S starts to act more like a fixed-wing aircraft, so a first/second-order system is a better fit, as shown in Figure 4.

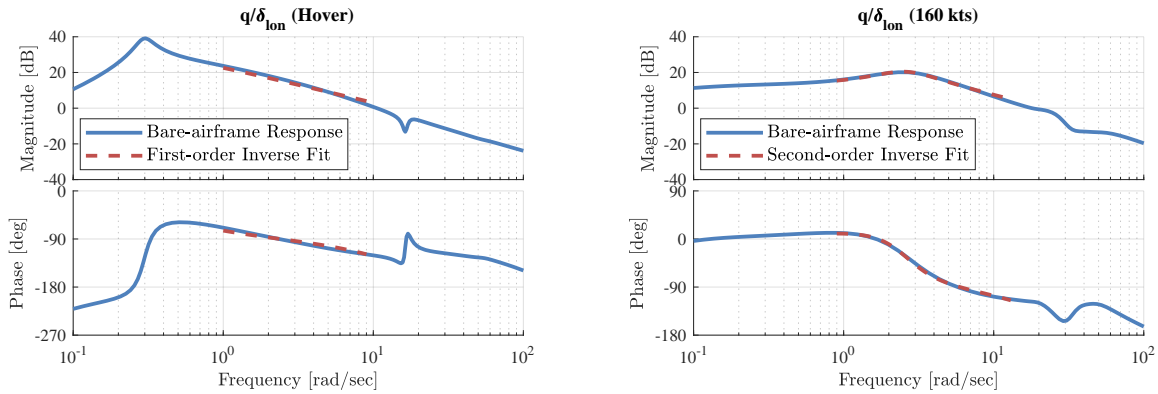


**Figure 4. Longitudinal axis inverse model fit at hover (first-order) and 160 kts (second-order).**

The pitch inverse model changes from first-order to first/second-order with a region of blending from 135 to 160 kts with the equations shown:

$$\frac{q}{\delta_{lon}} = \left( \frac{M_{\delta_{lon}}}{s - M_q} \right)_{\text{low airspeed}} \rightarrow \left( \frac{M_{\delta_{lon}}(s + 1/T_{\theta_2})}{s^2 + \zeta_{sp}\omega_{sp}s + \omega_{sp}^2} \right)_{\text{high airspeed}} \quad (2)$$

A similar change in dynamics exists in the yaw axis, where the same method of changing the inverse model with airspeed was employed. In the yaw axis, the change in dynamics, and therefore region of blending, starts at 50 kts and ends at 75 kts.

## 3. Equivalent Time Delay

An equivalent time delay  $\tau_\theta$  is included to account for inherent delays in the system and synchronizes the commanded states with the actual measured higher order response of the aircraft.<sup>21</sup> Delays in the system are typically from: actuators, sensors, filter, rotor flapping lag and other higher-order dynamics not canceled out by the the inverse model. Over the entire flight envelope, the calculated equivalent time delay in the pitch axis was between 0.02-0.06 seconds, 0.04-0.07 seconds in the roll axis and zero in the yaw axis.

## 4. Feedback

The feedback corrects for the residual modeling errors in the lower-order inverse approximation and is designed to provide stability and robustness. Along with good command model tracking, feedback effects the

gust rejection and hold capabilities, sensitivity to noise and disturbances and closed-loop damping of pilot and actuator inputs. Clearly, the feedback compensation is responsible for providing many competing requirements. A set of attitude rate, attitude, and attitude integral feedback gains was used in each axis to meet a comprehensive set of handling-qualities and flight control requirements.

## B. Inner-Loop Control Law Parameter Optimization

Feedback gains were optimized to meet a set of stability, handling-qualities and performance specifications using a multi-objective optimization method in CONDUIT<sup>®</sup>. The pseudo inverse control allocation was used in the optimization to allocate the redundant control effectors, details on the pseudo inverse will be provided in Section IV.A.

### 1. Specifications

The specifications can be divided into two Tiers, where the First Tier specifications are key in driving the optimization and the Second Tier are checked once the optimization is complete.<sup>21</sup> First Tier requirements can be broken into three categories: 1) *Stability*, 2) *Handling Qualities*, and 3) *Performance*. For an optimized design, these specifications are guaranteed to be met. To select the ADS-33E specifications for the X-49S, it is classified as a medium utility rotorcraft with MTE boundaries for moderate agility, visual meteorological conditions and fully attended operations (VMC and FAO). The set of stability, handling-quality, and performance specifications used for X-49S control system design are shown in Table 1 and example results for the hover flight condition are shown in Figure 5.

**Stability Requirements** In order to ensure a stable design with sufficient stability margins the following specifications were enforced: absolute eigenvalue stability (EigLcG1), gain and phase stability margins (Stb-MgG1), and Nichols margins (NicMgG1). Stability margins boundaries were set to require a gain margin  $\geq 6$  dB and a phase margin  $\geq 45$  deg for the full speed range based on recommendations in Ref. 21. The broken-loop feedback response  $\delta_{fb}$ , associated with the stability margins are based on breaking the loop at the input to the control allocation  $\delta_{mx}$  and is in terms of control axes: roll, pitch, yaw, shown in Figure 3.

**Handling Qualities Requirements** The model following specification (ModFoG2) is implemented to ensure good command model tracking in each axis. This specification computes the cost based on a weighted difference in magnitude and phase of the closed-loop response compared to the command model frequency response. To maintain handling qualities during disturbances, the disturbance rejection bandwidth (DrbReG1) and peak (DrpAvG1) specification are enforced in all the axes.

A key characteristic to the feedback design, the crossover frequency  $\omega_c$  is defined as the frequency for which the broken-loop response crosses the 0 dB line. The inner-loop crossover frequencies are determined like the stability margins, by breaking the loop at the input to the control allocation and is in terms of control axes (e.g. roll crossover frequency  $\omega_{c_\phi}$ ). Minimum crossover frequency requirements are enforced in each axis so that the control system is robust during uncertainty. The integral gain is constrained so that it is effective at holding trim and ensuring steady-state tracking, but not so large that it degrades the phase margin.<sup>21</sup> In each axis, the integral to proportional gain ratio was constrained at  $\omega_c/5$ , as suggested by Ref. 21.

The bandwidth (e.g. BnwRoH2) and maximum achievable rate (e.g. MaxRoH2) requirements were selected based on airspeed. The damping ratio of the closed-loop eigenvalues was evaluated to ensure it met the minimum required values (EigDpG1). The Open Loop Onset Point (OLOP) criterion evaluates the potential for sustained limit cycle oscillations due to actuation rate saturation for pilot and disturbance inputs. This specification is enforced for the equivalent main rotor servos and rudder. Because the X-49S has redundant surfaces, the OLOP criterion for the other aerosurfaces were also checked, but not enforced.

**Performance Requirements** Crossover frequency (CrsLnG1) and actuator RMS (RmsAcG1) specifications are used for performance optimization to minimize the control usage and drive down the amount of feedback, while the design still meets all the stability and handling qualities requirements. Actuator activity

is measured by the root mean squared (RMS) of the actuator displacement to a disturbance input. By including crossover frequency as a performance objective as well as a minimum requirement, the crossover will be high enough to provide consistent responses when variations or uncertainties occur, but low enough as to not drive up the actuator activity and decrease stability margins.

**Table 1. First tier control system specifications**

Specification	Description	Axis*	Speed [KIAS]
<i>Stability Requirements</i>			
EigLcG1	Eigenvalues	All	All
StbMgG1	Gain Phase Margin	All	All
NicMgG1	Nichols Margins	All	All
<i>Handling Qualities Requirements</i>			
ModFoG2	Command Model Following Cost	All	All
DrbReG1	Disturbance Rejection Bandwidth	All	All
DrpAvG1	Disturbance Rejection Peak Att./Vel.	All	All
MnxRoH1	Minimum Crossover Frequency $\omega_c \geq 3$ rad/sec	R	All
MnxPiH1	Minimum Crossover Frequency $\omega_c \geq 3$ rad/sec	P	All
MnxYaH1	Minimum Crossover Frequency $\omega_c \geq 4.8$ rad/sec	Y	All
BnwRoH2	Bandwidth and Time Delay	R	0-40
BnwRoF2	Bandwidth and Time Delay	R	80-180
BnwPiH2	Bandwidth and Time Delay	P	0-40
BnwPiF2	Bandwidth and Time Delay	P	80-180
BnwYaH2	Bandwidth and Time Delay	Y	0-40
BnwYaF1	Bandwidth and Time Delay (relaxed)	Y	80-180
MaxRoH2	Maximum achievable roll rate	R	0-40
MaxRoF2	Maximum achievable roll rate	R	80-180
MaxPiH2	Maximum achievable pitch rate	P	0-40
MaxPiF1	Maximum achievable pitch rate (relaxed)	P	80-180
MaxYaH2	Maximum achievable yaw rate	Y	0-40
MaxYaF1	Maximum achievable yaw rate (relaxed)	Y	80-180
EigDpG1	Damping Ratio	All	All
OlpOpG1	OLOP Criteria, pilot inputs	All	All
OlpOpG1	OLOP Criteria, disturbance inputs	All	All
<i>Performance Requirements</i>			
CrsLnG1	Minimize Crossover Frequency	All	All
RmsAcG1	Actuator RMS	All	All

\* R = Roll, P = Pitch, Y = Yaw

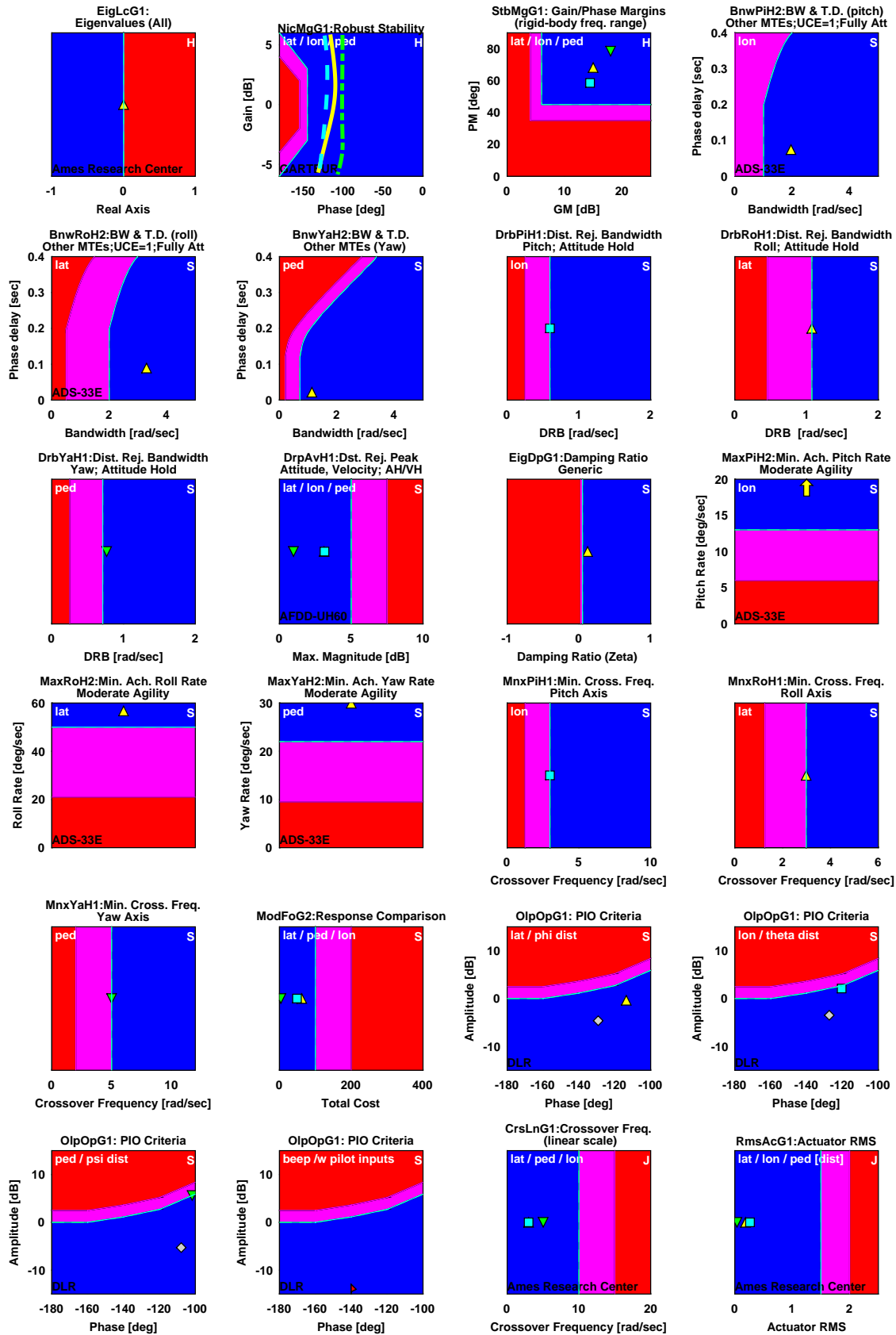


Figure 5. X-49S control system design specifications and results at hover in CONDUIT linear environment.

## 2. Gain Schedule

The control law parameters are comprised of the tuned command model parameters, equivalent time delays, inverse model parameters determined from low-order approximations, and the optimized feedback gains. The control law parameters for command model, equivalent time delays and inverse model were gain scheduled as a function of airspeed in 20 kt increments from hover to 180 kts. Feedback gains were optimized in 40 kt intervals from hover to 120 kts with a final point at 180 kts.

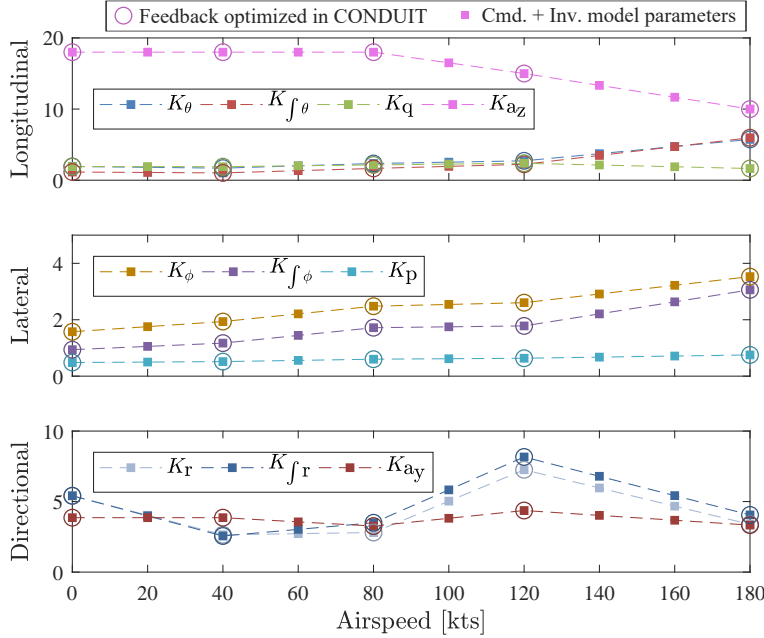


Figure 6. Feedback gains for X-49S over the speed envelope.

Figure 6 shows the gain schedule for feedback gains as a function of airspeed, where the optimized gains are circled and connected to show the linear interpolation used by the lookup tables of control laws. The smoothness in the interpolations demonstrate that the optimization resulted in smooth gain schedules and gave confidence that design points had adequate spacing (not too far apart).

## C. Outer-loop Control Laws

The X-49S FBW control system incorporates a number of outer-loop control functions, including: heading hold, airspeed hold, and barometric altitude hold. Only two outer-loop control functions were used in this study as discussed below.

### 1. Turn Coordination

The yaw axis controller includes a turn coordination controller that operates at airspeeds above 50 kts. In this mode, the yaw axis becomes a lateral acceleration command  $A_{y_{cmd}}$  / turn coordination response type. This was achieved via an outer-loop control law that produces a computed yaw rate command  $R_{cmd}$  for the inner-loop control law. The computed yaw rate command control law is derived from the lateral translation equation of motion as follows:

$$R_{cmd} = \frac{g[A_{y_{cmd}} + K(A_{y_{cmd}} - a_y) + \sin(\Phi)\cos(\Theta)]}{V_{tot}} \quad (3)$$

where the commanded lateral acceleration is proportional to the pilot pedal displacement.

## 2. SCS Mode

The X-49S control laws include a Speed Command System (SCS) control law that is designed to achieve and hold a commanded airspeed set by the pilot via a beep switch on the collective stick. The VTDP propeller pitch is the control effector used by the SCS to control airspeed. The system uses a schedule of nominal propeller pitch versus airspeed coupled with a simple proportional and integral feedback compensation on airspeed. The VTDP propeller has a torque limit that is highly sensitive to propeller pitch, so a torque limiting feedback loop is also included in the SCS. This loop takes over when the torque limit becomes critical. The SCS was used on some the damage scenarios in order to hold airspeed at an approximately constant set point, so that evaluations of the various configurations would be consistent.

# IV. Damage Tolerant Control Methods

## A. Control Allocation

### 1. Overall Methodology

In a traditional single main rotor helicopter, only 4 controls are available – lateral cyclic, longitudinal cyclic, main rotor collective pitch and tail rotor collective pitch. As such, redundancy is not available as all four controls are needed to maneuver the aircraft in the four control axes – pitch, roll, yaw and heave. In contrast, the X-49S compound helicopter has multiple redundant control effectors, as described earlier in this paper. These redundancies create non-unique solutions for controlling the aircraft. In order to achieve a desired commanded response, a strategy must be employed to determine which control actuators to use, and in what proportion. This strategy is called control allocation. By performing control allocation automatically in the flight control system software, it can also be ensured that the optimal proportion is used. The method of allocating the control determines the actuator position and rate required to meet the desired control moment, which in turn affects actuator position and rate saturation and associated ability to track the command. In the case that there is a failure of an actuator, control can be reallocated to other control effectors to maintain control over the aircraft until the aircraft can land safely, providing damage tolerant control (DTC). There are three control allocation methods that were evaluated:

- Nominal (not damage tolerant)
- Pseudo Inverse
- Quadratic Programming

The following sections of the paper describe each of these methods.

### 2. Nominal

The nominal control law does not use any special control allocation in the primary flight control law. The roll, pitch, and heave axes are controlled via cyclic and collective pitch as on a conventional helicopter. The yaw axis is controlled via the rudder and propeller using a prescribed mixing schedule (the "virtual walking beam" as discussed earlier). All control effectors may be used for aircraft trim, via manual slew switches by the pilot. However, only the primary controls listed above are used in the feedback control laws and for dynamic maneuvering of the aircraft. As such, this method has no failure reconfiguration capability other than the pilot adjusting their control compensation strategy based on the observed aircraft response.

### 3. Pseudo Inverse (DTC Method)

The pseudo inverse, is a method that uses the  $B$  matrix of the linearized aircraft dynamics to solve for the control actuator inputs  $u$  needed to supply the commanded change in the control force/moment  $\Delta d$ :

$$B\Delta u = \Delta d \quad (4)$$

where  $\Delta u = u - u_{pref}$ . The preferred control position  $u_{pref}$  represents the desired location of the actuator at trim. In the case that there are no saturation limits on the control inputs, the pseudo inverse provides

the linear solution that solves for the allocation that provides the desired moment while minimizing the L2 norm of the control input vector  $\|\Delta u\|_2 = [\Delta u]^T[\Delta u]$ . The form of the pseudo inverse is<sup>10,26</sup> :

$$\Delta u = B^T(BB^T)^{-1}\Delta d \quad (5)$$

It is also possible to use a weighted pseudo-inverse to put more weight on certain control effectors:

$$\Delta u = W_u^{-1}B^T(BW_u^{-1}B^T)^{-1}\Delta d \quad (6)$$

This solution does not utilize information about the position or rate saturation limits of the actuator and cannot compensate for saturation. In the case of saturation, the command is simply clipped by port limits, and the solution is no longer optimal. However, pseudo-inverse is able to reallocate in case of failure to provide damage tolerant control. For this work, we assume that any failures are known/detected, and do not address the work or algorithms needed to determine if a failure has occurred. In the case of failure, the column of the B-matrix associated with the failed actuator is simply set to zero and the preferred control effector positions vector  $u_{pref}$  is set to the failed position of the actuator in the case of a hard-over or frozen actuator.

#### 4. Quadratic Programming (DTC Method)

Quadratic programming is an optimization method that solves for the optimal (minimum cost) control allocation that provides the desired moment/acceleration within the position and/or rate limits of the actuators. This direct optimization method iteratively solves for the constrained optimization solution, at each time step.<sup>11,26,27</sup> This method will produce an exact solution in the case of actuator limiting, if a solution exists. However, there is no guarantee that the optimization will achieve the optimal solution in the desired time step. In the approach taken herein, the optimization based control allocation problem is fully convex. A very simple but powerful algorithm, Alternating Direction Method of Multipliers (ADMM) is used to solve the convex optimization problem at each time step.<sup>28</sup> The code to implement this method is very short and efficient, and as such was implemented by simple MATLAB S-functions. A maximum of 40 iterations were used to ensure that the solution can run in real time. Although an optimal solution is not guaranteed, the solution was found to be near optimal by Ivler in Ref. 8. Even with the simple efficient ADMM algorithm, additional computation time and complexity is required to implement this non-deterministic control allocation method. Failure reconfiguration is simply performed by setting the column in the B-matrix associated with the actuator to zero and setting the trim/preferred actuator position  $u_{pref}$  to the failed position. Then, the quadratic programming will still try to find a solution within the position and rate limits of the actuators as best possible under the failure conditions. The optimization takes the form:

$$\begin{aligned} &\text{minimize } J \\ &\text{where } J = \|W_u u\|_2 = (W_u u)^T(W_u u) \end{aligned} \quad (7)$$

**Subject to :**

$$B\Delta u = \Delta d$$

$$u_{min} \leq u \leq u_{max}$$

$$\dot{u}_{min} \leq \dot{u} \leq \dot{u}_{max}$$

where  $\Delta u = u - u_{pref}$ .

## B. Desktop Linear Simulation Results

### 1. Weighting matrix

Several different weighting matrices  $W_u$  were explored as part of the evaluation of the DTC system. It was determined via desktop evaluation that the weighting matrix affects the results of the DTC and also affects limiting behavior. The first evaluation of weighting was performed without the damage tolerant

control to determine that the aerodynamic control surfaces were properly used. Three weighting schemes were evaluated. The first weighting scheme was the baseline weighting:

$$\mathbf{W}_1 = \mathbf{I} \quad (8)$$

It should be noted that the B-matrix used in the allocation is converted to units of percent prior to performing control allocation so this baseline weighting is such that all control surfaces are represented in the same units. The second weighting scheme was a secondary weighting on the limits of the control effectors (typically called Bryson's Rule<sup>21</sup>):

$$\mathbf{W}_2 = 100 * \text{diag} \left( \frac{1}{\mathbf{u}_{max} - \mathbf{u}_{min}} \right) \quad (9)$$

applied to the solution where the B-matrix that has already been converted to units of percent. The third weighting scheme de-weights the aero-control surfaces and weights the main rotor servos four times as heavily as all other control surfaces:

$$\mathbf{W}_3 = \begin{bmatrix} 4 & 0 & 0 & 0 \\ 0 & 4 & 0 & 0 \\ 0 & 0 & 4 & 0 \\ 0 & 0 & 0 & \mathbf{I} \end{bmatrix} \quad (10)$$

applied to the solution where the B-matrix that is already been converted to units of percent.

The weightings were tested at several speeds. Large control inputs at 160 kts were used to evaluate the three weighting functions. At this condition, the weighting significantly affected the use of the rotor versus use of the aerodynamic surfaces, and saturation characteristics. Figures 7-9 show the actuator usage of the aircraft for a 50% pilot longitudinal stick input for each of the three weightings applied to the pseudo inverse and quadratic programming allocation methods. The nominal allocation is not affected by the weightings and so the traces are identical in all three figures. It should be noted that the effective main rotor control inputs are converted to pilot input units (lat, lon, col), which are back calculated from the main rotor servos, as these plots are easier to understand as compared to the main rotor servo coordinates. Additionally, the figures show the usage of the aerodynamic surfaces (rudder/pedal, two elevators and two flaperons).

Figure 7 shows the response to a large amplitude pitch doublet with weighting  $W_1$ . This weighting features the heavy use of the main rotor and light use of the aero-surfaces, as indicated by the small elevator inputs. It should be noted that the y-axis limits correspond with the limits of the actuator, so relative size can be directly compared. As shown in Figure 7, this weighting resulted in saturation of the main rotor for the pseudo inverse case, as shown by the effective longitudinal stick input to the main rotor. It is clear that a heavier use of the elevator could have avoided this saturation for the pseudo inverse case. For the quadratic programming case, we can see that the actuator just grazes the saturation limit, meeting the constraint, by adding an abrupt small downward input in to elevator at  $\sim 7$  sec. While this technically avoids saturation, the quadratic still grazes the limit, as it provides the best cost function with this weighting, similar to pseudo inverse, to use the longitudinal stick more heavily and then the saturation constraint only reallocates to the elevator if absolutely necessary.

The second weighting scheme  $W_2$ , shown in Figure 8, has a much more balanced use of the main rotor and elevator. We can see in this case, no saturation occurs. It should be noted that since no saturation occurs, the quadratic programming solution and pseudo inverse solutions are identical. This is expected as they both minimize the same cost function. The quadratic programming should only differ from the pseudo inverse if saturation occurs and those constraints become active.

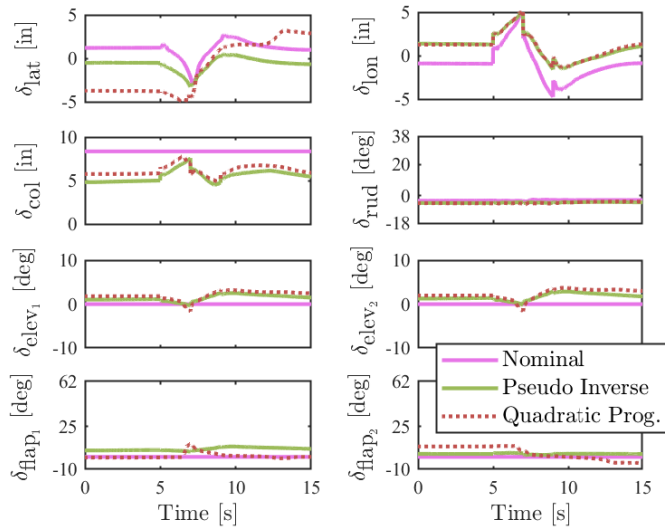


Figure 7. Weighting scheme 1  $W_1$ , 50% pitch doublet at 160kts

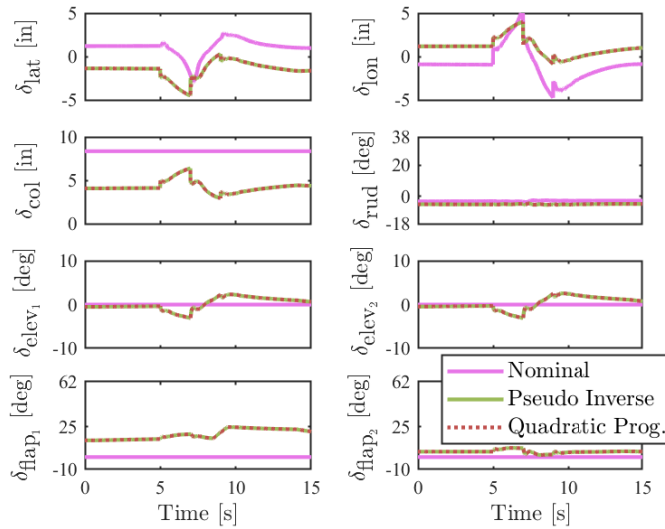


Figure 8. Weighting scheme 2  $W_2$ , 50% pitch doublet at 160kts.

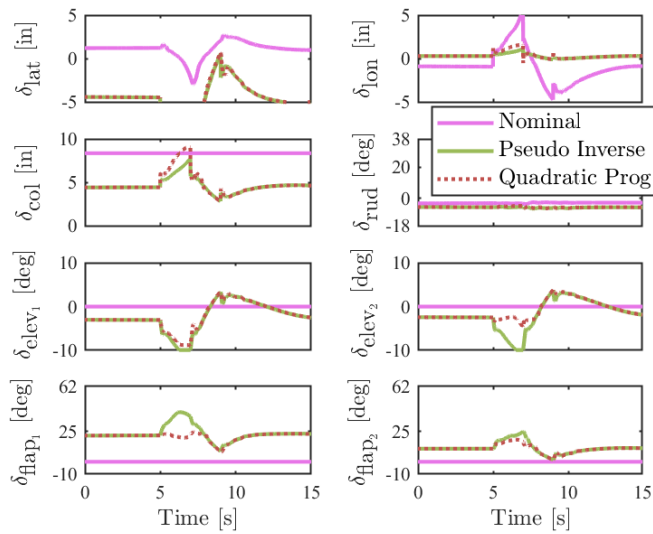


Figure 9. Weighting Scheme 3  $W_3$ , 50% pitch doublet at 160kts.

For the third weighting scheme  $W_3$  shown in Figure 9, the balance moves toward more use of the elevators, and less use of the stick. It should be noted that since the cost weighting is technically on the main rotor actuator, and not the effective stick inputs, the large lateral stick input is an artifact of that - where this particular reduction of the lateral stick will reduce the main rotor servo input. Still, it can be seen that this solution is not ideal, as the pseudo inverse begins to saturate and the usage of the elevators is very large. It can be seen that in regions of saturation the pseudo inverse and quadratic programming differ, where the quadratic programming reallocated to avoid saturation.

The pitch responses for all three weightings are compared in Figure 10. As shown in the figure, the rate responses are similar for all the cases, although  $W_2$  has better tracking of the command model in the positive peak response of the doublet, that occurs  $\sim 7$  sec. Overall, the second weighting  $W_2$  provided the best balance of actuator and aero-surface usage, and a slightly improved pitch rate response by avoiding saturation, even for this large and sharp doublet input. For all results in the following sections of this paper,  $W_2$  is used.

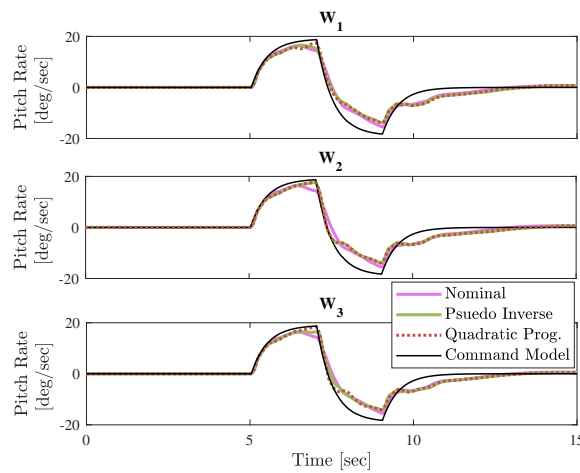


Figure 10. Pitch rate response to 50% pitch doublet for the three weighting schemes.

## 2. Verification of Control Allocation Functionality

After selecting the weighting, it was important to test the failure reconfiguration functionality to ensure that it was working properly. As mentioned earlier, once a failure is detected, the associated control derivatives of the failed actuator are set to zero in the allocation algorithm, so that the control is distributed only to functioning actuators. The preferred control position is set to the faulty actuator's position in order that the other controls can compensate for the forces and moments generated by the failure.

Example results for failure of the forward main rotor servo at 120 kts can be seen in Figure 11, where the forward main rotor servo is frozen at  $\sim 1.6$  inches for all control allocation methods. At about 5 seconds into the record, a small pitch doublet is input to the system. The nominal control allocation, which only uses the aero-surfaces for trim, is not able to compensate for this failure, resulting in large oscillatory lateral and aft main rotor servo inputs. The pseudo inverse and quadratic programming are able to compensate for the failed control by utilizing the aero-surfaces.

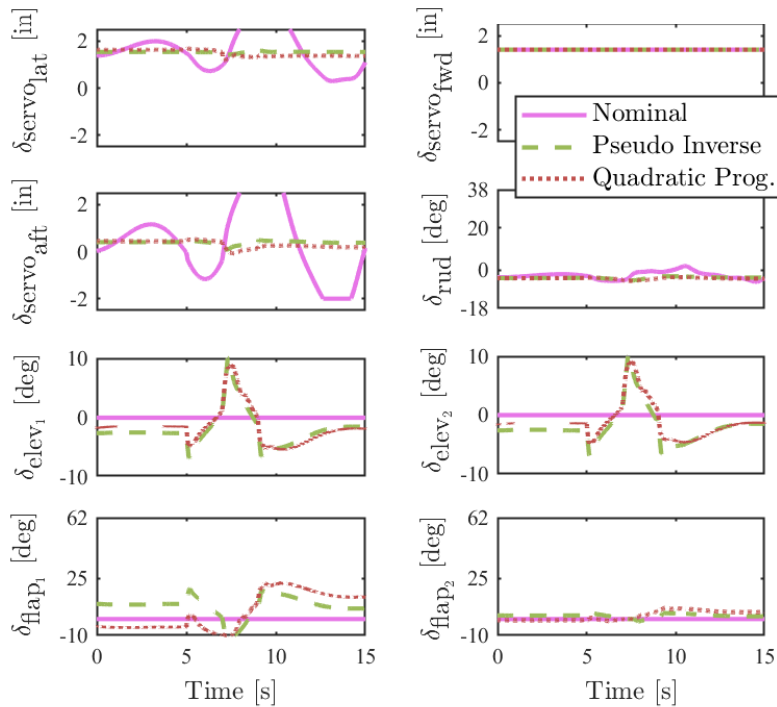


Figure 11. Actuator responses with forward main rotor failure, 20% pitch doublet at 120kts.

For the nominal case, the associated response of the aircraft is oscillatory and unstable as shown in Figure 12. However, the pseudo inverse and quadratic programming methods are both able to successfully recover from this failure. As shown in the actuator responses of Figure 11, most of the control allocation is redistributed to the elevators under the failure conditions. In addition, both these damage tolerant control allocation methods can still track the commanded pitch rate, as shown in Figure 12. Similar tests of the other actuator failures were performed to verify the damage tolerant control functionality.

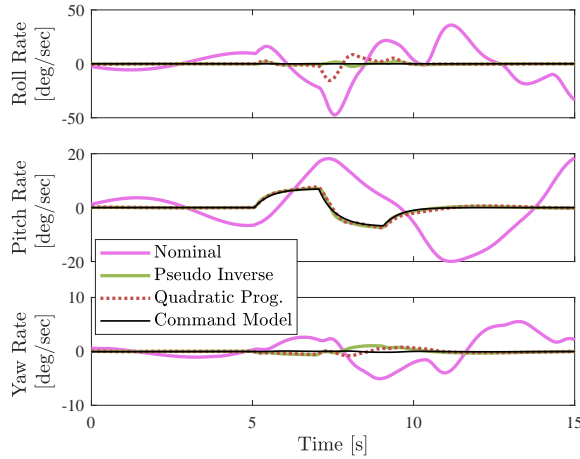


Figure 12. Attitude rate response with forward main rotor failure, 20% pitch doublet at 120 kts.

### C. Adaptation with Neural Network

An adaptive augmentation element is included, as shown in Figure 3, to address faults where we would like the vehicle to continue to track the reference model to the extent possible through online modification of the feedback and feed forward gains. This could happen with or without a reconfiguration of the control allocation. Therefore, some faults would not require control reconfiguration to be handled. In prior work, the approach includes an online trained artificial neural network to correct a dynamic inversion control law.<sup>29</sup> For this research, the formulation is applied to an explicit model following control law; which is an important difference. Figure 13 illustrates the controller with the proposed augmentation as the “adaptive element”. Note that this augmentation appears almost like integral action but, it is an integral action that is state dependent. This means that it can generate nonlinear state feedback to drive the system to reference model dynamics.

In this design, it is possible to map control system design parameters (the linear feedback gains and parameters associated with the nominal model) in such a way that existing stability results for neural network adaptive controllers directly apply (e.g., Ref. 29). This means that a controller with this design will be on the same solid analytical footing as prior work. To illustrate the method, consider the simple reproduction of an idealized roll axis response, where a simple model is used for the true roll motion (first order lag to roll rate, a consistent structure with the inverse model in the explicit model following design). We have also included parameter error in the model to exercise the adaptation in the presence of a degradation. As shown in Figure 14, the aircraft is successively rolled left and right. The adaptive parameters converge to correct values over time, allowing the model following design to improve performance.

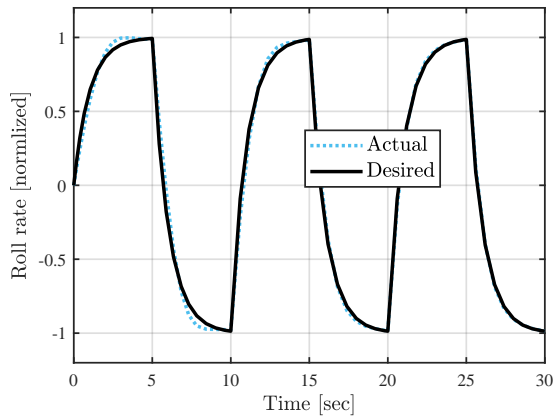


Figure 13. As adaptive gains converge, the roll reference model and actual roll eventually coincide (normalized by maximum rate).

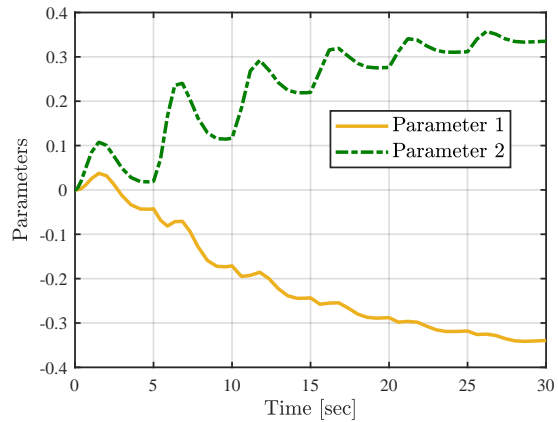


Figure 14. Example of two adaptive parameters, both reaching steady state once adaptation is complete.

## V. Piloted Simulation

### A. Simulation Facility

The X-49S was flown in the Penn State Vertical Lift Center of Excellence Fixed-Base Simulator. This simulator is composed of the cab and cockpit of an XV-15 tiltrotor, featuring conventional helicopter controls (cyclic, collective, and pedals) with additional buttons, switches, and touchscreen controls available for the additional control effectors, shown on the left in Figure 15. A four-channel control loading system reads the cockpit stick positions and allows for fully-programmable high-bandwidth control loading. Outside displays are driven using a three-channel high-resolution projection system on a 15-foot diameter by 11-foot high cylindrical screen with image generation from X-Plane professional flight simulation software, shown on the right in Figure 15.



Figure 15. Cockpit inceptors and displays (left) and flight simulation facility (right).

## B. Test Plan and Task Descriptions

The simulation testing was performed using the Cooper-Harper Handling Qualities Rating Scale (Figure A1) and the Sullivan Survivability Ratings Scale (Figure A2) to evaluate four controllers: 1) Nominal, 2) Pseudo Inverse, 3) Quadratic Programming and 4) Pseudo Inverse with Neural Network Adaptation in the feedback loop. The maneuvers flown are described below and presented in Table B.

**Table 2. Simulation Test Matrix**

Maneuver	Speed [KIAS]	Altitude [ft AGL]	Axis* (R/P/Y)	Rating Type†	Damage Type‡	No. Pilots
Validation Sweeps	60, 120, 180	200	All	-	-	-
High Speed Break Turn	150	200	-	HQR	-	4
High Speed Capture/Hold	150	2000	P	HQR	-	3
	150	2000	R	HQR	-	3
	150	2000	P	HQR	Aft	1
High Speed SOS Tracking	150	2000	P	HQR	-	3
	150	2000	R	HQR	-	3
	150	2000	P	HQR	Aft	3
	150	2000	R	HQR	Aft	3
Damage Scenario	0-120	0-300	-	SR	Aft	3
	0-120	0-300	-	SR	Fwd	3
	0-120	0-300	-	SR	Lat	3
	0-120	0-300	-	SR	Prop	3
	0-120	0-300	-	SR	Tail, 5% eff.	3
	0-120	0-300	-	SR	Tail, 20% eff.	1

\* R = Roll, P = Pitch, Y = Yaw † HQR = Handling Qualities Ratings, SR = Survivability Rating  
‡ Aft, Fwd, Lat = aft, forward and lateral main servo failures, Prop = prop drive shaft failure, Tail = tail damage with  $X\%$  rudder effectiveness

During the simulation testing of handling qualities and damage survivability evaluation, pilots were not informed on which controller (or control allocation) was active. For the flight with damage, the pilot was informed which damage case was active (forward, aft or lateral main rotor servo, prop drive shaft, or VTDP damage). However, for the VTDP damage case, the pilot was not informed of the severity of the damage (quantified as rudder effectiveness). The pilot was informed by the simulator operator when the damage was activated, in case it was not apparent in the aircraft response.

### 1. Handling Qualities Tasks

The maneuvers that were given handling qualities ratings (HQRs) were the High Speed Break Turn,<sup>18</sup> Sum-of-Sines Tracking<sup>17</sup> and Attitude Capture/Hold.<sup>16</sup> The selection of these specific maneuvers was intended to investigate any potential handling qualities issues, cliffs, bobble, cross coupling, maneuverability limitations, or pilot induced oscillation (PIO) tendencies. These recently developed maneuvers are designed to evaluate rotorcraft that perform at high speeds. The current high-speed MTEs in ADS-33E were newly vetted in terms of standardized parameters and cuing requirements; in 2019, flight tests of the maneuvers were performed to refine the test maneuvers.<sup>30</sup>

Descriptions of the maneuvers are provided in Ref. 16–19. Once the handling qualities of the aircraft with various controllers was evaluated, the pitch capture/hold and pitch and roll tracking MTEs were reflight with the aft main rotor servo damaged. With these flights, the ability of each controller to re-allocate control effectively using redundant effectors can be evaluated.

## 2. Damage Tolerance Survivability Task

Each damage case was flown in order to determine pilot workload and survivability of the damage for each of the controllers. For these flights, after the damage was activated, pilots were instructed to regain control of the aircraft, followed by a climbing left turn (at 30 degree of bank angle) and descending right turn; these turns were included to exercise the redundant control effectors. After the turns, the pilot was instructed to complete an approach and landing in a suitable area. Since the redundant control effectors lose aerodynamic effectiveness at low airspeeds, the pilot was permitted to perform a run-on landing. Pilot workload and damage survivability were evaluated by the pilot after each flight using the Sullivan Survivability Scale (Figure A2). This 5-point scale, with 1 representing most survivable and 5 representing least survivable, uses 3 questions to determine a rating, similar to the Cooper-Harper HQR scale (Figure A1). The questions evaluate whether the pilot was able to attempt an immediate emergency landing, whether the pilot could continue flight to return to base or another location, and whether the pilot could land within the aircraft limits (in the case of the X-49S, below 60 kts forward velocity, loss of attitude control of less than 10 deg in all axes, and less than 540 ft/min rate of descent for a run-on landing).

### C. Control System Validation

In order to validate the implementation of the nonlinear simulation model, dynamic checks were performed at three flight conditions: 60, 120 and 180 kts. Automated frequency sweeps were injected into the pilot controls, and frequency responses were checked against linearized models. An example of the closed-loop frequency responses are shown in Figures 16 and 17. As expected, all the control allocation methods achieve the same closed-loop linear responses. These responses matched the linearized models of the closed-loop system used in control optimization and batch testing.

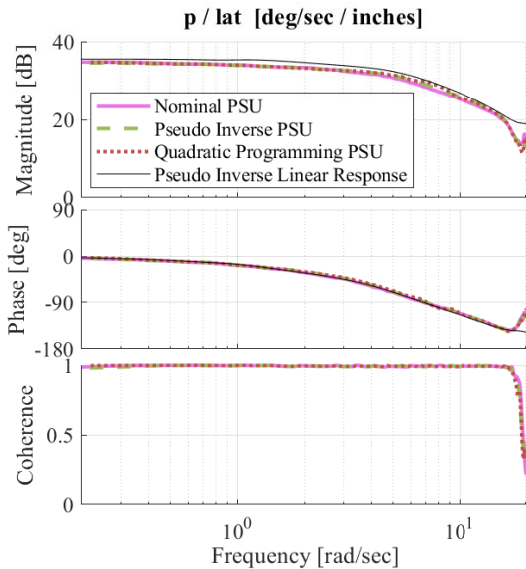


Figure 16. Frequency domain validation of PSU simulation compared to linear response roll axis at 120 knots.

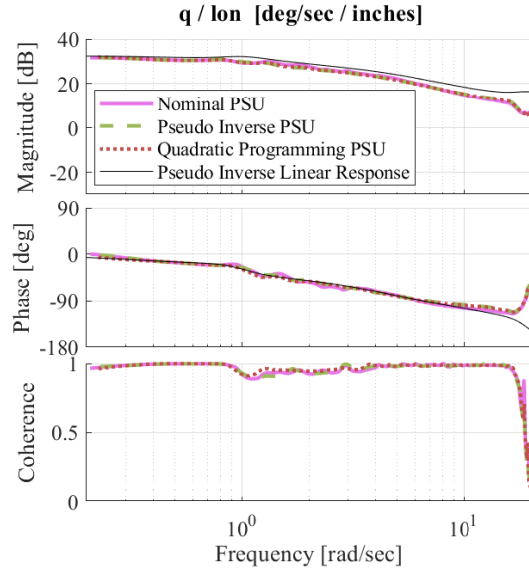


Figure 17. Frequency domain validation of PSU simulation compared to linear response pitch axis at 120 knots.

### D. Piloted Simulation Test Results

The overall Handling Qualities Ratings (HQR) and Survivability ratings are shown in Figure 18, where the average ratings of each controller are reported. One can see that the handling qualities ratings of the various controllers are very similar when there is no damage. When damage was simulated, the controllers that reconfigured for damage almost always out performed the nominal control allocation. Due to the many maneuvers flown, the results section focuses on the most interesting and notable outcomes.

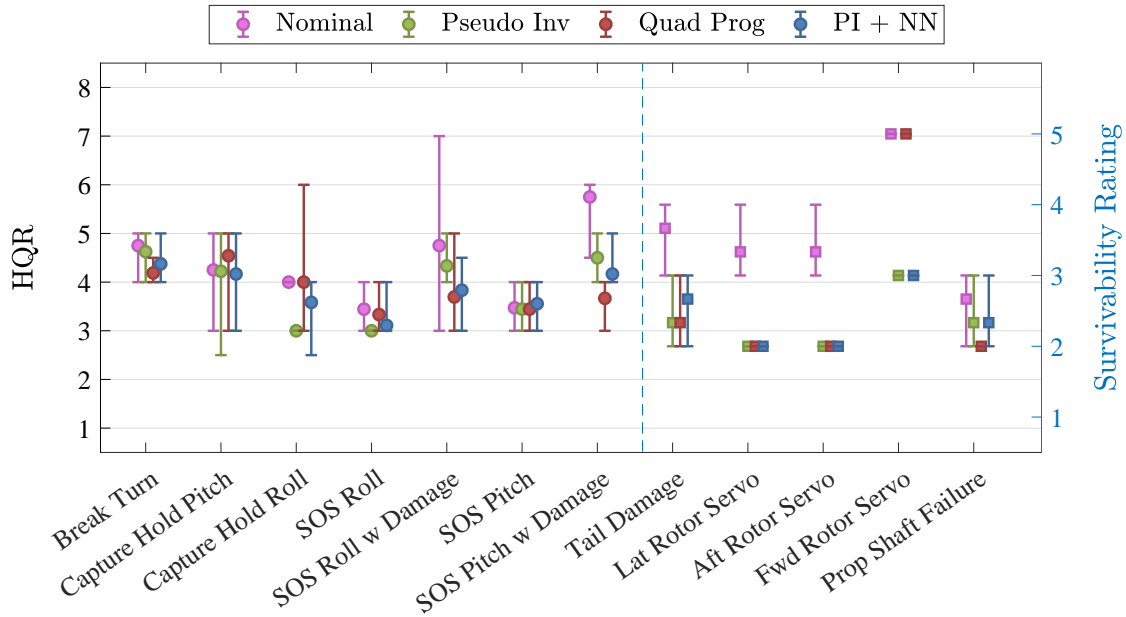


Figure 18. Overall piloted simulator ratings.

### 1. High Speed Break Turn Results

The damage tolerant methods provide some benefits in normal operating conditions because they are control allocation methods that can be used to distribute the control across all the actuators, reducing saturation and potentially improving handling qualities. The handling qualities ratings for the high speed break turn are shown in Figure 19. As shown in the figure, the results were within one HQR for all control allocation

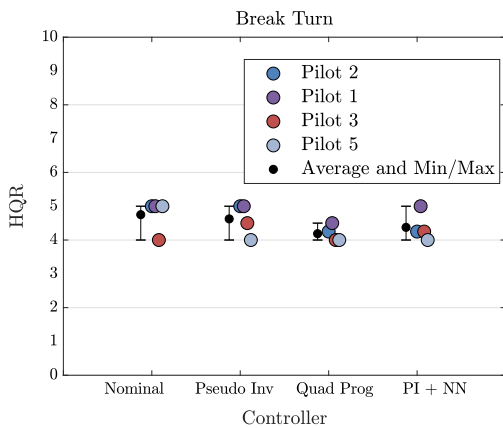


Figure 19. Pilot HQRs for high speed break turn.

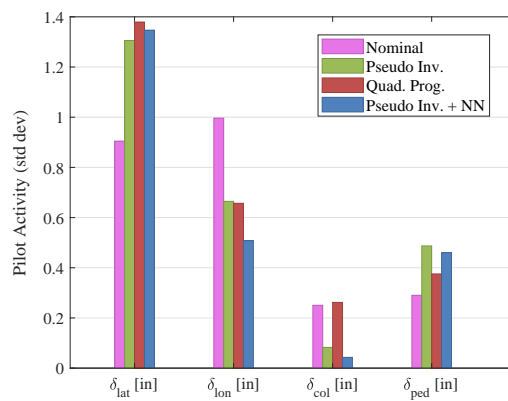


Figure 20. Variance in pilot effector activity during high speed break turn.

methods. However, it should be noted that quadratic programming method and pseudo inverse with neural network methods provided slightly better than average ratings, than the nominal control allocation with the worst average rating. Although the differences between the damage tolerant methods and the nominal methods are small in the HQRs, from Figure 20 it appears that pilots flew the maneuver with less variance in lateral cyclic and more longitudinal cyclic with the nominal allocation as compared to the DTC methods.

The DTC methods used the symmetric elevators in favor of main rotor servos, shown in Figure 21, which likely was the cause of the nominal allocation’s higher variance in hub moments in Figure 22. Note that the selected weighting for flaperon control did not result in larger flaperon deflections in nominal conditions. However, flaperon usage increases significantly in damage scenarios.

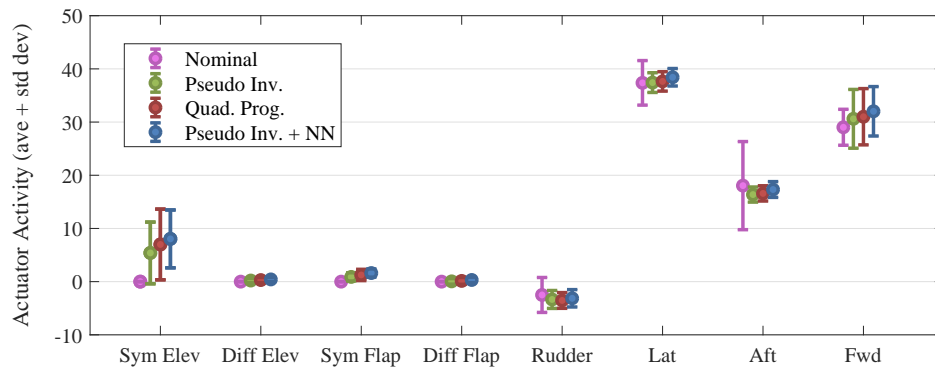


Figure 21. High speed break turn actuator activity.

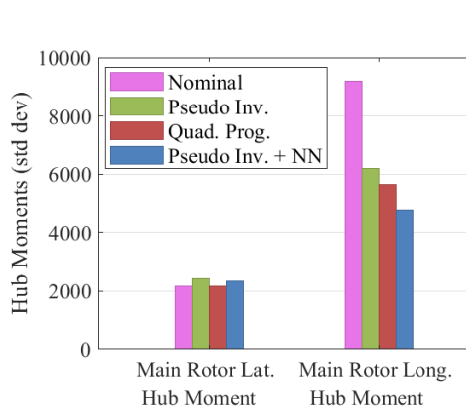


Figure 22. Hub moments during high speed break turn.

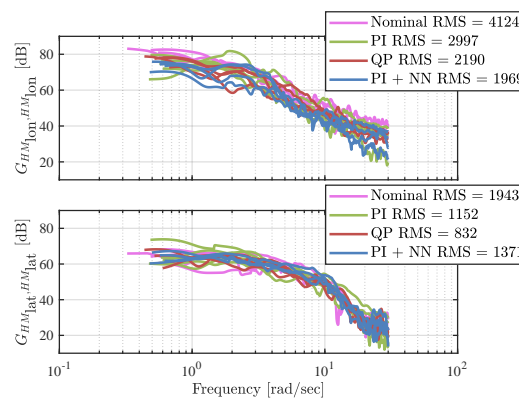


Figure 23. Autospetra of hub moment during high speed break turn.

Figure 23 shows that nominal allocation has significantly higher average hub moments RMS values, but there is no significant difference between the damage tolerant methods. For the nominal allocation case, there is more use of the aft main rotor servo and associated hub moments, as shown in Figure 21, because the nominal allocation method does not allocate the flaperon and elevator aerosurfaces. The use of aerosurfaces, which have a faster response time at high speeds, over the rotor, could be advantageous in an aggressive maneuver like the break turn, and could be related to the slight degradation of HQR for nominal allocation.

## 2. Attitude Capture/Hold Results

The simulation results for the bank angle capture hold task found that pilots generally felt that the nominal control allocation was the worst, although this is not completely supported by the HQR ratings shown in Figure 24. Pilots commented that more off-axis input was needed to accomplish this task with the nominal allocation, one stated that it required “more work in pitch.”

The trace in Figure 25 shows a time history from the poor rating of quadratic programming, it was originally an HQR 3, but the pilot adjusted his rating to a 6 based on the scoring criteria for deviating outside of the acceptable region in the second capture and the extensive pilot workload needed to capture attitude. When flying the quadratic programming allocation, one pilot commented that he had to “struggle

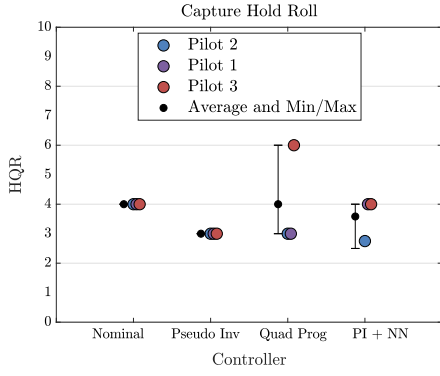


Figure 24. Pilot HQRs for bank angle capture hold.

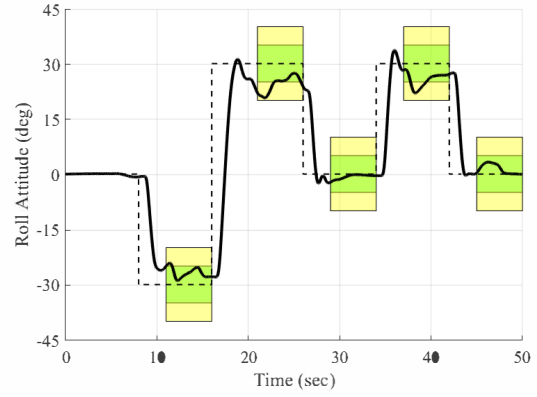


Figure 25. Time history of the bank angle capture hold task flow with quadratic programming by Pilot 3.

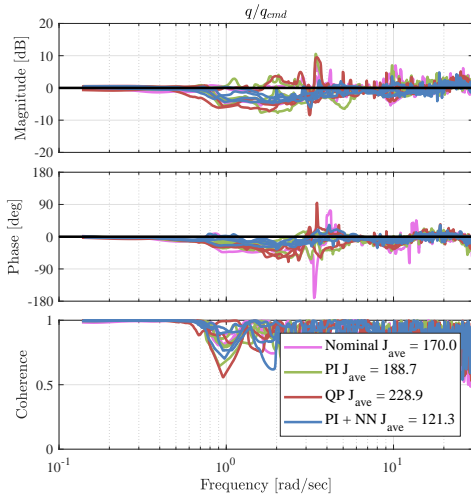


Figure 26. Pitch (off-axis) model following during bank angle capture hold.

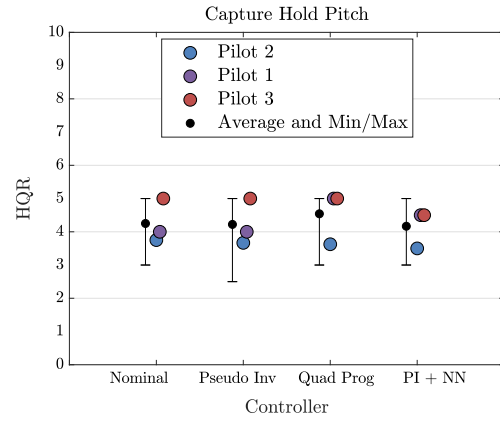


Figure 27. Pilot HQRs for pitch attitude capture hold.

to capture and hold bank angle.” Figure 26 shows the off-axis pitch model following during the maneuver for all the records with HQRs. The average cost  $J_{ave}$  for the response to commanded input (command model with time delay) are given for each controller. The cost is calculated as defined in Reference 31:

$$J = \frac{20}{n_\omega} \sum_{\omega_{min}}^{\omega_{max}} [1.58(1 - e^{-\gamma_{xy}^2})]^2 [W_g(|D|)^2 + W_p(\angle D)^2] \quad (11)$$

$|D|$  is magnitude [dB] at each frequency  $\omega$

$\angle D$  is phase [deg] at each frequency  $\omega$

$\gamma_{xy}^2$  is coherence at each frequency  $\omega$

$n_\omega$  is number of frequency points

$W_g$  is relative weight for magnitude squared-error

$W_p$  is relative weight for phase squared-error

where  $D$  is the error-response and for this case it is the frequency response of actual to commanded attitude rate, evaluated from a minimum frequency  $\omega_{min}$  of 0.3 rad/sec to maximum frequency  $\omega_{max}$  of 12 rad/sec,

and with the conventional 1-dB magnitude error to 7.57-deg phase error weighting. As shown in Figure 26, quadratic programming control allocation had a significantly higher average cost than the other allocation methods. The poor off-axis model following may have contributed to why pilots struggled to hold the bank angle, and played a role in one poor HQR for the quadratic programming controller.

The simulation results from pitch attitude capture hold task did not vary significantly between controllers, based on Figure 27. Although pilots seemed to agree that quadratic programming had a “higher workload post-capture [hold] than others, seems less predictable.” Overall, pilots preferred the pseudo inverse and pseudo inverse with neural network controllers.

### 3. Sum-of-Sines Tracking Results

The sum-of-sines tracking task in roll resulted in similar handling qualities ratings for all the control allocation methods, as shown in Figure 28, the aircraft requires minimal to moderate pilot compensation for desired performance. Pseudo inverse and pseudo inverse with neural network had slightly more favorable HQRs, needing less pilot compensation than quadratic programming and nominal allocation methods. No major differences in performance between the control allocation methods were evident until the maneuver was flown with damage.

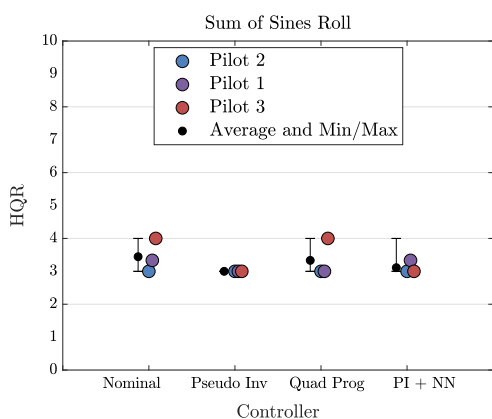


Figure 28. Pilot HQRs for roll sum-of-sines tracking.

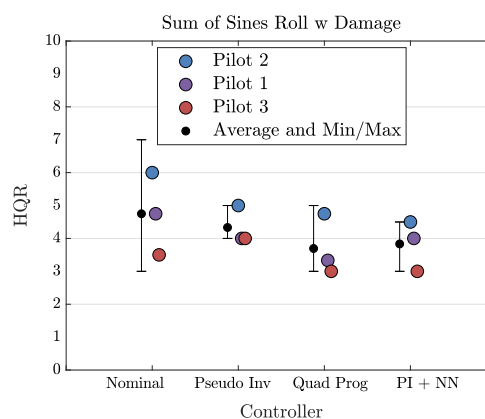


Figure 29. Pilot HQRs for roll sum-of-sines tracking with damage.

Flying the maneuver with an aft servo failure generally drove up the average handling qualities ratings, see Figure 29. The servo failure had less of an impact on HQRs for the DTC methods, especially the quadratic programming and pseudo inverse with neural network controllers, which appeared to only slightly degrade pilot ratings relative to the case without damage. The pilot handling qualities ratings correlated fairly well with their tracking performance, supported by Figure 30. This figure compares the average percentage of the run that the pilot flew within the desired performance limits (at least 50% of scoring time is within  $\pm 5$  deg attitude error in roll) versus the average handling quality rating given by each pilot for each of the controllers. The light markers with HQRs around 3 flown without damage had a wider range of tracking performance between 56-72%. Whereas the darker, open markers with higher HQRs and slightly lower performance represent the tracking task flown with damage. Figure 30 shows that DTC methods achieved better pilot ratings and performance compared to the nominal control allocation. Overall the performance with and without damage did not differ greatly, likely because of the pilot was able to compensate for reduction in pitch control sensitivity with the aft servo damage, and the task was primarily in the roll axis.

In addition to the task performance analysis, pilot-vehicle system performance was analyzed using the data from three of the test pilots. Given the known input forcing function, pilot-vehicle system  $Y_p Y_c$  describing functions were computed for all of the roll and pitch sum-of-sines tracking task runs with and without damage. References 17 and 30 provide detailed descriptions of this process. Figure 31 shows the nearly identical pilot-vehicle systems for the control allocation methods in roll during the roll tracking task. As

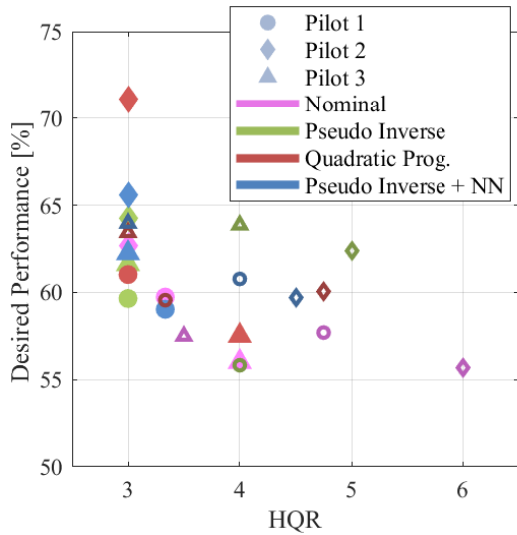


Figure 30. Roll sum-of-sines tracking performance versus average handling qualities ratings of each pilot.

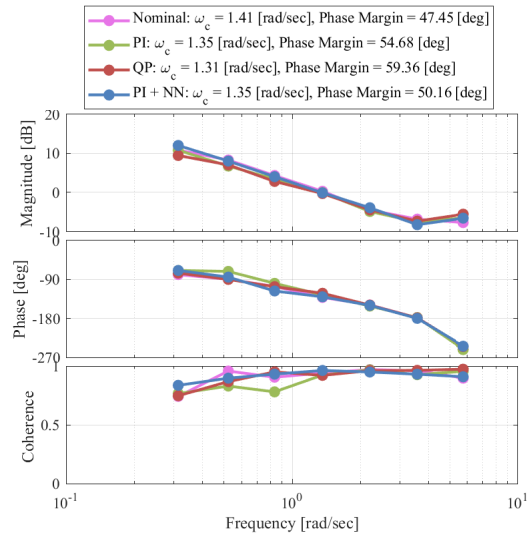


Figure 31. Pilot-vehicle system  $Y_p Y_c$  in roll from sum-of-sines tracking task.

expected, the magnitude of the pilot-vehicle system responses follow a  $k/s$ -like behavior in the region around crossover (0 dB). The pilot-vehicle system responses were also computed for the runs with damage, shown in Figure 32. These pilot-vehicle system responses appear to differ and one might assume this means the performance of the controllers differed. Figure 32 shows that in general, the crossover frequencies degraded and phase margin increased with damage, with the exception of quadratic programming.

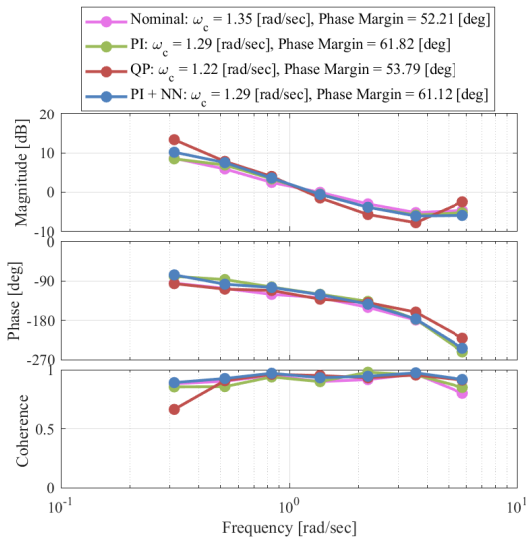


Figure 32. Pilot-vehicle system  $Y_p Y_c$  in roll from sum-of-sines tracking task with damage.

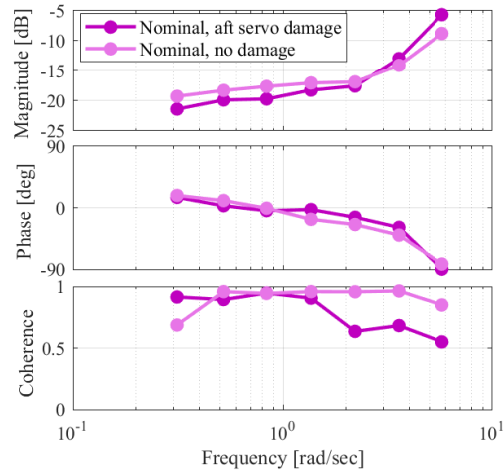
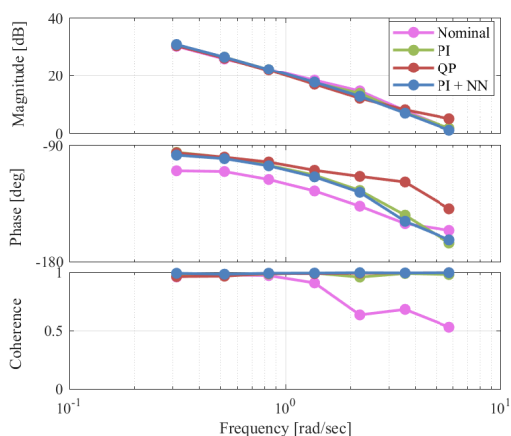


Figure 33. Comparison of pilot models  $Y_p$  in roll from sum-of-sines tracking task with nominal control allocation with and without damage.

Lower crossover frequencies and higher phase margins would indicate that the pilots tended to back out of the loop, likely preferring to trade performance for overall stability. However, the slight decrease in crossover frequencies did not necessarily indicate a significant change in task performance, as demonstrated in Figure 30. From analyzing the pilot models for each of the allocation methods, it appears that pilots

tended to back out of the loop and compensated for the damage by adding lead. This is evident in looking at the pilot model responses in Figure 33 where an example of the pilots response using nominal allocation with and without damage are compared. The pilot models with nominal allocation were shown because these models most dramatically demonstrated this trend.

To better isolate whether the control allocation methods or the pilots contributed to the change in performance of the pilot-vehicle systems, the aircraft models  $Y_c$  were computed. The aircraft models appeared to be identical for all the allocation methods when the tracking task was flown without damage. Figure 34 reveals that during the aft servo failure, the control allocation methods affect the aircraft model of the system or aircraft performance. The aircraft response with nominal allocation lags the other responses, which is apparent in the phase response in Figure 34. The quadratic programming control allocation aircraft response led that of pseudo inverse controllers, this is likely the cause of the small lead at higher frequencies of the pilot-vehicle system with quadratic programming control allocation.



**Figure 34. Aircraft model  $Y_c$  in roll from sum-of-sines tracking task with damage.**

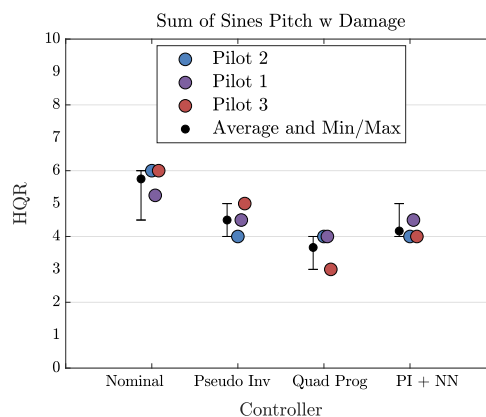


**Figure 35. Pilot HQRs for pitch sum-of-sines tracking with damage.**

As with the roll axis, the sum-of-sines tracking task in pitch resulted in similar handling qualities ratings for all the control allocation methods. Repeating the tracking task with damage helped to differentiate between the control allocation methods. Pilot HQRs varied dramatically between control allocation methods as shown in Figure 35. Pilots rated quadratic programming, pseudo inverse with neural network, pseudo inverse and lastly nominal control allocation, in order of best to worst HQRs. The pilots' handling qualities ratings correlated well with the tracking performance, supported by Figure A3, where the higher performance and best handling qualities ratings tend toward the top right and degraded performance and ratings tend toward the bottom right. The aft servo failure appeared to have little to no effect on performance for quadratic programming. The pseudo inverse with and without the neural network had similar performance with and without damage. For all the control allocation method except quadratic programming, these results are consistent with the computed frequency domain analysis of the pilot-vehicle system.

As in the roll axis, the pilot-vehicle systems for the control allocation in pitch were all fairly similar with crossovers of  $\sim 1.9$  rad/sec and phase margins of  $\sim 42$  deg. Figure A4 shows the pilot-vehicle systems for the pitch tracking task flown with damage. For the pseudo inverse, pseudo inverse with neural network and nominal control allocation methods, the damage resulted in pilot-vehicle systems with higher crossover and much less phase margin. This reflects the pilots likely increased compensation in response to the sluggish response that resulted from damage. From the computed aircraft response from aft servo damage, presented in Figure A5, the phase delay is evident, except in quadratic programming. When the pilot-vehicle system and aircraft model for quadratic programming with and without damage were compared they look almost identical. By looking at the actuator activity in Figure A6, it appears that the quadratic programming algorithm reallocated more of the elevator, which could be why the aircraft model with quadratic programming has more lead.

#### 4. Main Rotor Servo Failure Results

The survivability ratings for the three main rotor servo failure cases had very different results. For the forward main rotor servo failure, survivability ratings were best for the pseudo inverse with and without neural network cases as shown in Figure 36. The quadratic programming method did not provide an improvement over the nominal control allocation, both resulted in nearly immediate loss of control. Unlike the nominal control allocation, quadratic programming worked well in the linear simulation that featured linear model dynamics at a single airspeed and associated fixed main rotor servo limits. Quadratic programming likely did not perform well in the piloted simulation that has full nonlinear dynamics due to the complexities of the saturation limits in the main rotor servos, which have biases that change as a function of flight condition for each of the servos, resulting in minimum and maximum position limits that change with airspeed. As such it was difficult to apply the constraints effectively in maneuvering flight for the quadratic programming. Perhaps this could be improved in the future, but it does speak to the fragility of the method with variable actuator limits and complexity of implementation. This is confirmed by the rate saturation that occurs for the quadratic programming method, as shown in Figure 38, which means that the quadratic programming is not functioning properly for this failure.

In contrast with the forward main rotor servo failure results, the aft servo failure showed little difference between the DTC methods, with all three having significantly improved survivability ratings as compared to the nominal method, as shown in Figure 37. The difference as compared to the forward servo may be attributable to the location of the servo failure, which was less severe. The lateral main rotor servo had similar results, where the DTC methods showed similar advantages over the nominal control allocation in terms of hub moments, actuator usage and model following.

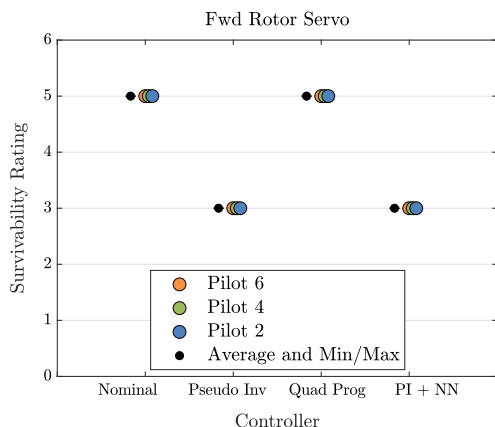


Figure 36. Pilot survivability ratings for forward main rotor servo failure.

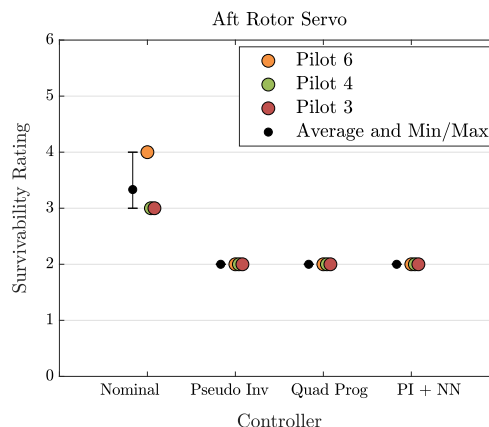


Figure 37. Pilot survivability ratings for aft main rotor servo failure.

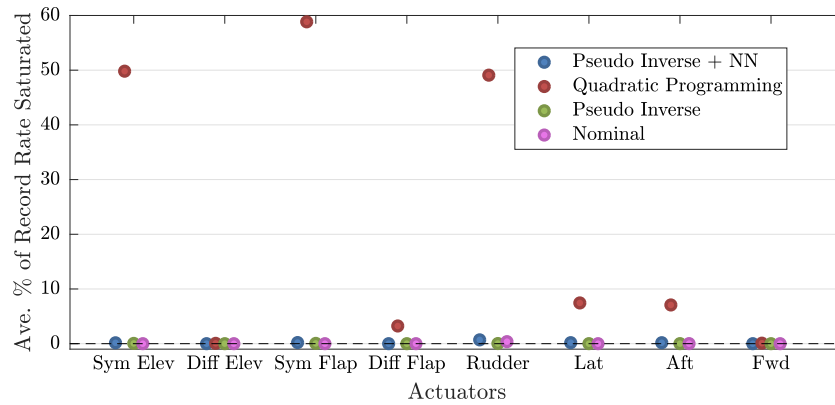


Figure 38. Rate saturation during forward main rotor servo failure.

### 5. Tail Damage Results

The tail damage case simulates loss of partial functionality of the rudder such that only 5% of the surface effectiveness is available. The reason for simulating this condition as opposed to full loss of the tail is that there are no other yaw control effectors. In the case of full loss of the tail, the aircraft is not controllable. For the 5% rudder effectiveness case, the damage tolerant methods are aware of the failure as well as the rudder effectiveness. This method is effective in improving the survivability rating over the nominal case, as shown in Figure 39. The quadratic programming and pseudo inverse were most effective at mitigating this failure. The presence of the neural network did not improve the damage tolerance over the pseudo inverse without neural network in this case. As seen by the rate saturation during the record in Figure 40, the pseudo inverse with neural network had increased rate limiting as compared to the quadratic programming and pseudo inverse cases, which might be attributable to the poorer survivability ratings.

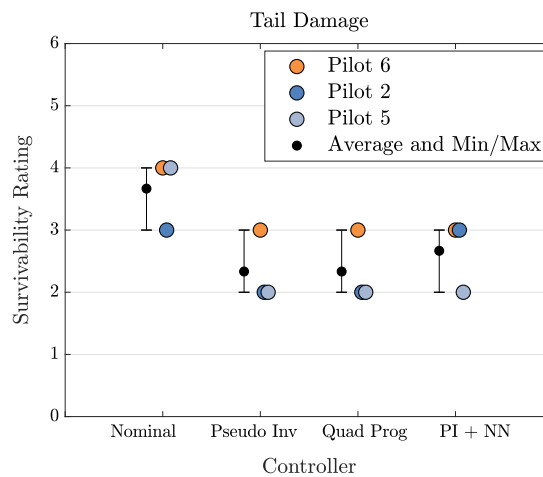


Figure 39. Tail damage survivability ratings.

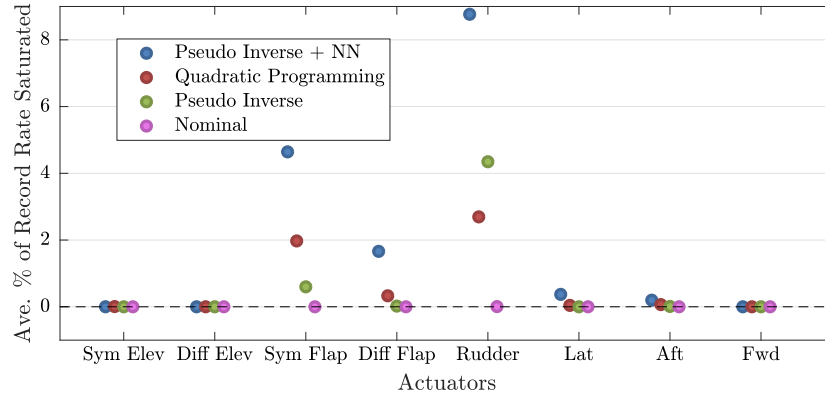


Figure 40. Actuator rate saturation with tail damage, 5% rudder effectiveness.

## VI. Discussion

This section will discuss overall results from the simulation testing and how well qualitative results from pilot ratings and comments correlate with the quantitative results from the flight data analysis. For the high speed break turn, the handling qualities ratings were fairly similar for all of the controllers, although pilots perceived that quadratic programming had the best and nominal (does not reallocate for damage) had the worst performance. Note that all of the break turns were performed without damage. Analysis of the flight data showed that pilots tended to use more off-axis pitch inputs to perform the task with the nominal control allocation method as compared to the other DTC methods. This additional off-axis input would likely mean pilots had increased workload, likely resulting in the slightly degraded HQRs. The data analysis generally found that the three DTC methods performed moderately better than the nominal control allocation method.

For the bank angle capture/hold task without damage, pilots generally gave more favorable handling qualities ratings to the DTC methods as compared to the nominal allocation method. Pilot comments on quadratic programming control allocation method regarding additional workload, this was also seen in the data analysis as poor off-axis tracking. For the pitch attitude capture/hold task, pilots commented that the quadratic programming controller required a higher workload for holding the target attitudes. However, the data analysis did not show significant differences between the controllers for the pitch task.

For the sum-of-sines tracking tasks in roll and pitch, pilots ratings were too similar to distinguish between the control allocation methods. Consistent with the pilot ratings, the frequency domain analysis of the pilot-vehicle systems for the control allocation methods looked identical. Overall, the handling qualities with DTC methods was comparable or better than those with the nominal allocation scheme. The nominal allocation scheme is expected to work well in cases without control saturation or damage, so this result is not surprising. Flying the sum-of-sines tracking MTE with main rotor servo damage resulted in a wider spread in the piloted ratings. In both roll and pitch, quadratic programming had the most favorable ratings, and all DTC schemes showed improvement (on average) over the nominal allocation.

For the survivability testing, pilots rated the pseudo inverse with neural network slightly worse than the other DTC methods during tail damage. This finding was supported by the data in terms of the rate saturation of the actuators. However, this might be mitigated by better tuning of the adaptive neural network. Note that the neural network attempts to force the aircraft to follow the model response, when a better approach might be to relax the command model instead of tracking the ideal model. All of the DTC methods had small amounts of rate saturation in the rudder and flaperons, however, pseudo inverse with neural network had the highest rate saturation percentages. Pilot ratings and quantitative analysis were consistent for the forward servo failure. Quadratic programming had a significant amount of rate saturation, which was the cause of the poor survivability. For the lateral and aft servo failures the DTC methods

had very similar, if not the same, pilot ratings and the quantitative data analysis showed very similar results.

For most of the tasks, the DTC methods were rated and performed better than the nominal control allocation method. However, some of the tasks flown did not produce an obvious superior control allocation method. In certain cases, the quadratic programming and the pseudo inverse with neural network controllers provided advantages but made the response worse in others. As such, the recommended controller is the pseudo inverse, which had good performance across all cases as compared to the nominal. The pseudo inverse improved survivability over the nominal allocation method for all failures tested and improved HQRs relative to nominal for the high speed MTEs. Of the DTC methods, the pseudo inverse had the lowest percentage of rate saturation and behaves the most predictably.

All of the DTC approaches showed improved survivability ratings over the nominal allocation schemes. In many cases, the aircraft could be landed within roll-on landing tolerances at a desired location when using the DTC methods. During the simulation setup for survivability testing it was observed that the test results and survivability of the aircraft were sensitive to failure severity. For example, the position at which the servos were failed significantly impacted the level of damage. Engineering judgement was used to set up the damage scenarios for reasonable and (ideally) realistic levels of severity. When setting up the simulation for tail damage, the initial percentage of rudder effectiveness was much larger and damage was essentially undetectable to the setup pilot. Therefore, the rudder effectiveness was decreased (more severe damage) so that the pilots could experience some amount of degradation in flying performance.

For the survivability damage scenarios, pilots flew a maneuver with loose guidelines. The analysis of the survivability was evaluated immediately after the fact, based on both the pilot's perception of survivability and the safety limits of the aircraft during landing. In rating the survivability in this way, the qualitative and quantitative results were closely tied. For the purposes of quantitatively analyzing the flight data, flying a specific, more well defined maneuver or track would have likely produced more repeatable data and potentially a survivability metric could be calculated (separate from the pilot rating). The survivability rating scale created for this research had many criteria that were specific to the aircraft's safety limits for run-on landings. For several of the damage scenarios, the speed at which the pilot landed greatly effected the survivability rating. At low airspeeds the advantages from the control allocation methods diminish greatly due to the loss of redundancy in effective aerosurfaces. Therefore, pilots would generally land at a slightly higher airspeed so as to avoid loss of control. Pilots suggested that the system should cue them during damage. For example, the system could alert the pilot when the aircraft is near a loss of control condition, particularly at low airspeeds, or warn the pilot that he/she must not reduce speed below a specified amount. Pilots commented that they would like the display system to inform them when the system was reacting to a failure.

The bank angle capture/hold MTE description details that the maneuver is be performed alternating the initial starting direction from left to right. However, it was observed that the initial direction had an effect on the ratings. This is likely because rolling to the right versus left have different amounts of pitch coupling. Pilots found that their control strategies also played a role in the HQRs. For example, when pilots were too aggressive this negatively impacted their performance and ratings. To mitigate these two factors and gather consistent ratings, the experiment used the same initial roll direction (instead of alternating) and the pilots tried to maintain a lower, more constant level of aggression.

The sum-of-sines tracking MTE allowed additional insight into the frequency response of the system. Not only was the pilot-vehicle system performance able to be analyzed, but aircraft and pilot models could be computed and evaluated separately to see how one effected the other. This was especially valuable when the tracking task was flown with damage because one could compute the pilot model and observe how pilot technique changed with and without damage. This MTE did an excellent job of exposing aircraft issues such as coupling and time delays. This was observed when the roll tracking task was flown with the nominal control allocation with damage, and the aircraft model had an additional time delay caused by the aft servo failure.

## VII. Conclusions

This paper described the development and handling qualities assessment of flight control systems for a winged compound helicopter. Overall, the survivability ratings and HQRs of the systems showed improvement with control allocation methods. Additionally, the damage tolerant capabilities of the control systems were assessed for multiple damage scenarios, where control allocation methods significantly improved aircraft survivability. This paper used a survivability rating scale which is a good starting point for evaluation of a system's damage tolerance performance. The following conclusions are drawn from this research:

1. At low speeds the improved survivability from the control allocation methods diminish greatly due to the loss of redundancy in effective aerosurfaces.
2. Evaluation of the control allocation methods using the high speed sum-of-sines tracking task MTE with damage was an effective method to evaluate damage tolerant performance and gain insight on the overall pilot-vehicle system.
3. Control allocation for damage tolerance was shown to be beneficial not only in damage scenarios but, also improved performance because using control allocation makes for faster responses, due to less actuator limiting and rate saturation.
4. More complex, non-deterministic damage tolerant methods like quadratic programming and neural networks showed great advantages in improving performance, but more tuning and work is required to ensure their reliability.
5. Many of the control allocation methods have advantages for specific situations, this research found that pseudo inverse was the most favorable damage tolerant controller for performance and reliability.

## Acknowledgments

The authors would like to thank the test pilots in the simulation study Doug Miller, Christopher Sullivan, LTC Carl Ott, Jim Wright, Craig Ernst and Grey Hagwood for providing their time, insight, and excellent comments. Furthermore, the authors would like to thank Joe Horn's students who helped run the simulator.

## References

- <sup>1</sup>Chase, N. A., "Future Vertical Lift Overview," American Helicopter Society International Specialists' Meeting on Rotorcraft Propulsion, Williamsburg, VA, October 2015.
- <sup>2</sup>Trimble, S., "US Army reveals details of Joint Multi-Role fleet vision," Flight Global, August 2011.
- <sup>3</sup>Hirschberg, M., "JMR Technology Demonstration Update: The Road to Future Vertical Lift," Vertiflite, Vol. 62, Issue 1, January 2016.
- <sup>4</sup>Bailey, D., "Joint Multi-Role Technology Demonstrator (JMR TD) Overview," American Helicopter Society, May 2015.
- <sup>5</sup>Couch, M. and Lindell, D., "Study on Rotorcraft Safety and Survivability," American Helicopter Society 66th Annual Forum, Phoenix, AZ, May 2010.
- <sup>6</sup>Berger, T., Juhasz, O., Lopez, M. J. S., Tischler, M. B., and Horn, J. F., "Modeling and Control of Lift Offset Coaxial and Tiltrotor Rotorcraft," European Rotorcraft Forum, Delft, The Netherlands, September 2018.
- <sup>7</sup>Sonneborn, W. G. O. and Hartwig, L. W., "Results of High-Speed Flight Research with the High Performance UH-1 Compound Helicopter," American Helicopter Society 27th Annual V/STOL Forum, 1971.
- <sup>8</sup>Ivler, C. M. and Juhasz, O., "Evaluation of Control Allocation Techniques for a Medium Lift Tilt-Rotor," American Helicopter Society 71st Annual Forum, Virginia Beach, VA, May 2015.
- <sup>9</sup>Durham, W. C., "Constrained Control Allocation," Journal of AIAA Guidance, Control, and Dynamics, 1992.
- <sup>10</sup>Oppenheimer, M., Doman, D., and Bolender, M., "Control Allocation Approaches for Over-Actuated Systems," Mediterranean Conference on Control and Automation Proceedings, Ancona, Italy, 2006.
- <sup>11</sup>Enns, D., "Control Allocation Approaches," Proceedings of AIAA Guidance, Navigation and Control Conference and Exhibit, 1998.
- <sup>12</sup>Piasecki Aircraft Corporation, "X-49A Scientific and Technical Final Flight Test Report," .
- <sup>13</sup>Geiger, B., Piasecki, F., Horn, J., Schifferle, P., and Lotterio, M., "Challenges of Flight Control in a Compound Helicopter," Proceedings of the International Powered Lift Conference, Philadelphia, PA, October 2010.
- <sup>14</sup>Piasecki Aircraft Corporation, "Piloted Simulation 1 Test Plan, Adaptive Digital Automated Pilotage Technology," 6-Y-301A, 2017.
- <sup>15</sup>Piasecki Aircraft Corporation, "Piloted Simulation 1 Outbrief, Adaptive Digital Automated Pilotage Technology," 6-Y-301B, 2018.

- <sup>16</sup>Klyde, D. H., Pitoniak, S. P., Schulze, P. C., Ruckel, P. D., Rigsby, J. M., Xin, H., Fegely, C. E., Fell, W. C., Brewer, R. L., Conway, F., Mulato, R., Horn, J. F., Ott, C. R., and Blanken, C. L., "Piloted Simulation Evaluation of Attitude Capture and Hold MTEs for the Assessment of High-Speed Handling Qualities," American Helicopter Society 74th Annual Forum, Phoenix, AZ, May 2018.
- <sup>17</sup>Klyde, D. H., Pitoniak, S. P., Schulze, P. C., Ruckel, P. D., Rigsby, J. M., Fegely, C. E., Xin, H., Fell, W. C., Brewer, R. L., Conway, F., Mulato, R., Horn, J. F., Ott, C. R., and Blanken, C. L., "Piloted Simulation Evaluation of Tracking MTEs for the Assessment of High-Speed Handling Qualities," American Helicopter Society 74th Annual Forum, Phoenix, AZ, May 2018.
- <sup>18</sup>Xin, H., Fegely, C. E., Fell, W. C., Horn, J. F., Ruckel, P. D., Rigsby, J. M., Brewer, R. L., Conway, F. P., Mulato, R., Klyde, D. H., Pitoniak, S. P., Schulze, P. C., Ott, C. R., and Blanken, C. L., "Further Development and Piloted Simulation Evaluation of the Break Turn ADS-33 Mission Task Element," American Helicopter Society 74th Annual Forum, Phoenix, AZ, May 2018.
- <sup>19</sup>Berger, T., Blanken, C., Tischler, M. B., and Horn, J. F., "Flight Control Design and Simulation Handling Qualities Assessment of High-Speed Rotorcraft," Vertical Flight Society 75th Annual Forum, Philadelphia, PA, May 2019.
- <sup>20</sup>Howlett, J., "UH-60A Black Hawk Engineering Simulation Program: Volume I - Mathematical Model," NASA CR 166309, December 1981.
- <sup>21</sup>Tischler, M. B., Berger, T., Ivler, C. M., Mansur, M. H., Cheung, K. K., and Soong, J. Y., *Practical Methods for Aircraft and Rotorcraft Flight Control Design: An Optimization-Based Approach*, AIAA, 2017.
- <sup>22</sup>Anon., "Handling Qualities Requirements for Military Rotorcraft," Aeronautical Design Standard-33 (ADS-33E-PRF), US Army Aviation and Missile Command, March 2000.
- <sup>23</sup>McRuer, D., Ashkenas, I., and Graham, D., *Aircraft Dynamics and Automatic Control*, Princeton University Press, 1990.
- <sup>24</sup>Tischler, M. B., Fletcher, J. W., Diekmann, V. L., Williams, R. A., and Cason, R. W., "Demonstration of Frequency-Sweep Test Technique Using a Bell-214-ST Helicopter," *NASA TM 89422, Army TM 87-A-1*, April 1987.
- <sup>25</sup>Ivler, C. M., "A Constrained State-Space Coupling Numerator Solution and Application to UH-60 Helicopter Control Design," *Journal of Guidance, Dynamics and Control*, Vol. 38, No. 10, October 2015.
- <sup>26</sup>Page, A. and Steinberg, M., "A Closed-Loop Comparison of Control Allocation Methods," Proceedings of AIAA Guidance, Navigation and Control Conference and Exhibit, Denver, CO, 2000.
- <sup>27</sup>Bodson, M., "Evaluation of Optimization Methods for Control Allocation," *Journal of Guidance, Navigation, and Control*, Vol. 25, No. 4, 2002.
- <sup>28</sup>Boyd, S., Parikh, N., Chu, E., Peleato, B., and Eckstein, J., "Distributed Optimization and Statistical Learning via the Alternating Direction Method of Multipliers," *Foundations and Trends in Machine Learning*, Vol. 3, No. 1, 2001, pp. 1–122.
- <sup>29</sup>Johnson, E. N. and Kannan, S. K., "Adaptive Trajectory Control for Autonomous Helicopters," AIAA Journal of Guidance, Control, and Dynamics, June 2005.
- <sup>30</sup>Berger, T., Ott, C. R., Reichelt, R., Cox, J., De Cecchis, P., and Wood, J., "Flight Test Assessment of High-Speed Mission Task Elements," Vertical Flight Society 75th Annual Forum, Philadelphia, PA, May 2019.
- <sup>31</sup>Tischler, M. B. and Remple, R. K., *Aircraft and Rotorcraft System Identification: Engineering Methods and Flight Test Examples Second Edition*, AIAA, 2012.

## Appendix of Figures

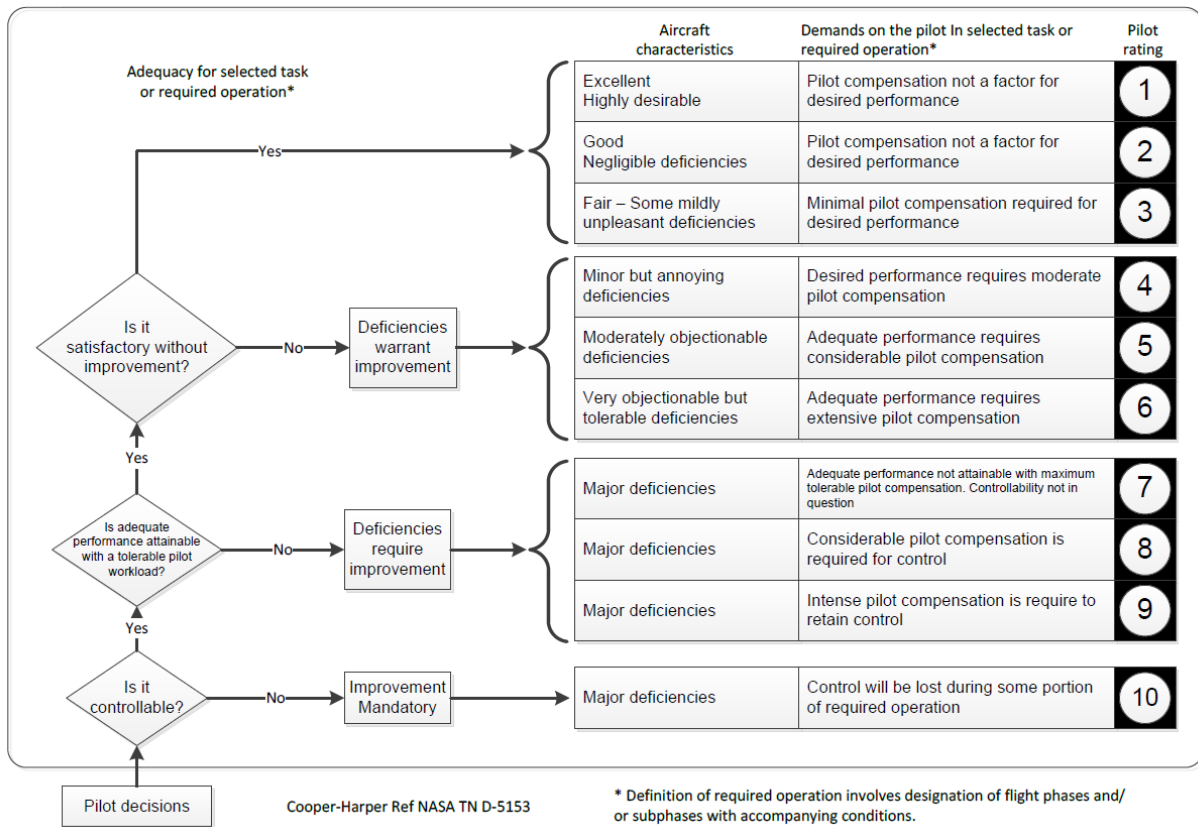


**Figure A1. Cooper-Harper Handling Qualities Rating Scale.**

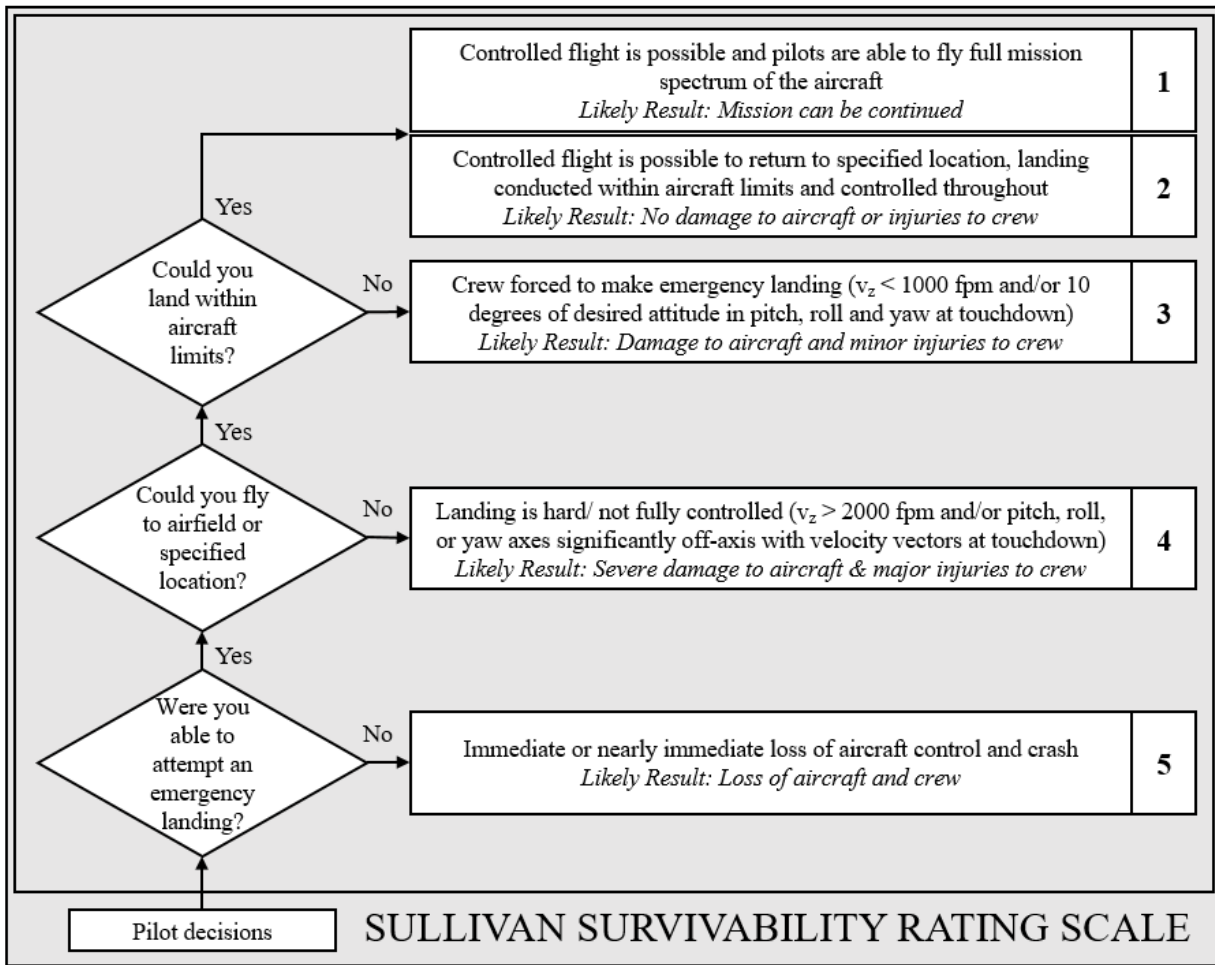


Figure A2. Sullivan Survivability Rating Scale.

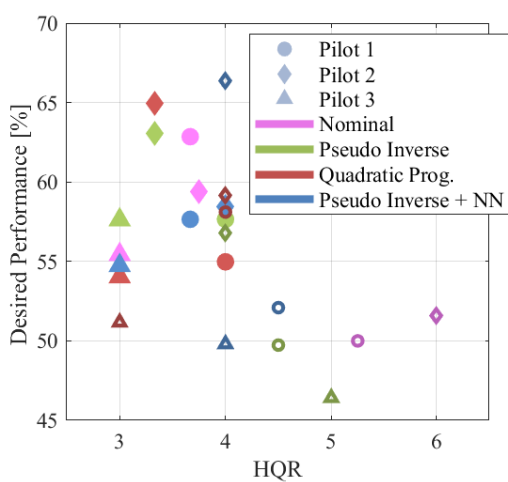


Figure A3. Pitch sum-of-sines tracking performance versus average handling qualities ratings of each pilot.

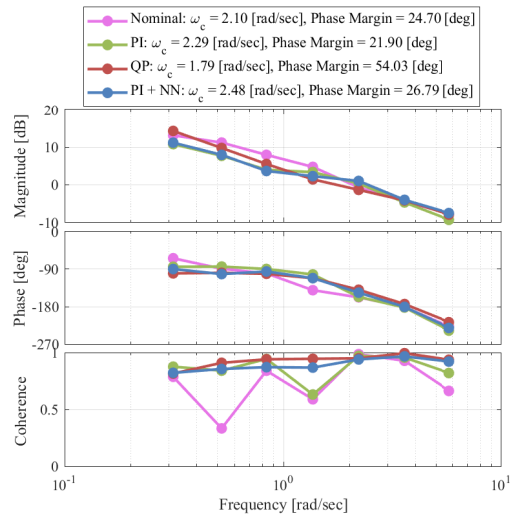


Figure A4. Pilot-vehicle system  $Y_p Y_c$  in pitch from sum-of-sines tracking task with damage.

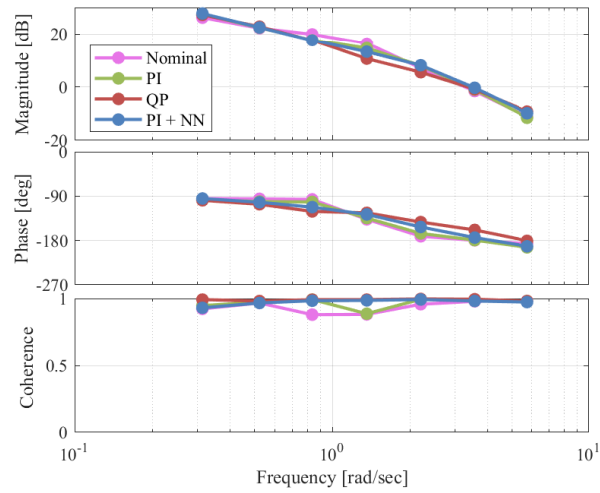


Figure A5. Aircraft model  $Y_c$  in pitch from sum-of-sines tracking task with damage.

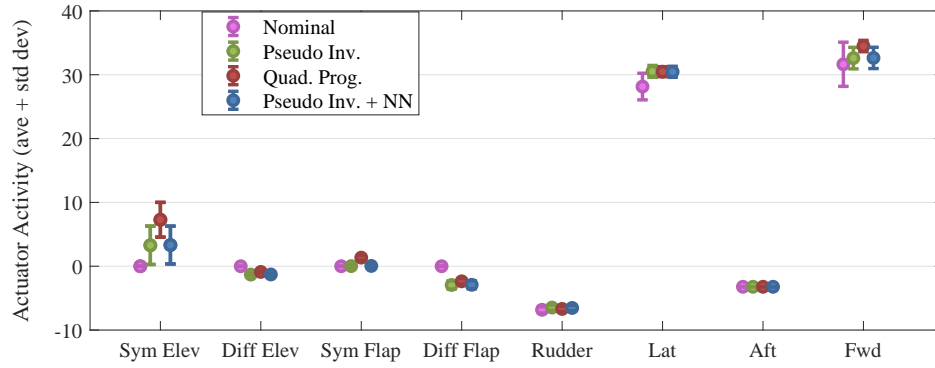


Figure A6. Actuator activity during sum-of-sines pitch tracking task with damage.